

Krylov Complexity in early universe

Ke-Hong Zhai and Lei-Hua Liu

Department of Physics, College of Physics, Mechanical and Electrical Engineering, Jishou University, Jishou 416000, China

E-mail: 2023700328@stu.jsu.edu.cn, liuleihua8899@hotmail.com

ABSTRACT: The Lanczos algorithm offers a method for constructing wave functions for both closed and open systems based on their Hamiltonians. Given that the entire early universe is fundamentally an open system, we apply the Lanczos algorithm to investigate Krylov complexity across different phases of the early universe, including inflation, the radiation-dominated period (RD), and the matter-dominated period (MD). Notably, we find that Krylov complexity differs between the closed and open system approaches. To effectively capture the impact of potentials during the RD and MD phases, we analyze various inflationary potentials—including the Higgs potential, the R^2 inflationary potential, and chaotic inflationary potential—taking into account the violations of slow-roll conditions. This analysis is conducted in terms of conformal time through the preheating process. Our numerical results indicate that the evolution of Krylov complexity and Krylov entropy is remarkably similar across both methods, regardless of the potential under consideration. Additionally, we rigorously construct what is referred to as an open two-mode squeezed state, utilizing the second kind of Meixner polynomials. Based on this construction, we are the first to calculate the evolution equations for r_k and ϕ_k as they relate to the scale factor. Our findings suggest that dissipative effects lead to a rapid decoherence-like behavior. Moreover, our results indicate that inflation behaves as a strongly dissipative system, while both the radiation-dominated and matter-dominated phases exhibit characteristics of weak dissipation. This research provides new insights into exploring the universe from the perspective of quantum information.

ARXIV EPRINT: [1234.56789](https://arxiv.org/abs/1234.56789)

Contents

1	Introduction	1
2	Lanczos algorithm with the approach of closed system	3
3	Some setup of early universe	4
3.1	Inflation, RD and MD	5
3.2	Various inflationary potentials	6
4	Evolution of two-mode squeezed state	8
4.1	Two-mode squeezed state	8
4.2	The evolution of $r_k(\eta)$ and $\phi_k(\eta)$	9
5	Krylov complexity in closed system	11
5.1	Krylov complexity	11
5.2	Krylov Entropy	13
6	Krylov complexity with the approach of open system	14
6.1	Lanczos coefficient and dissipation coefficient	14
6.1.1	b_n, c_n and μ_2	15
6.2	General discussion of ϕ_n	17
6.3	Wave function within the method of open system	17
6.4	The power of wave function (6.32)	20
6.5	The evolution of $r_k(\eta)$ and $\phi_k(\eta)$ in open system's method	20
6.6	Krylov complexity and Krylov entropy with the approach of open system	21
7	Summary and outlook	23
A	The calculation of r_k and ϕ_k within the method of open system	27

1 Introduction

The idea of complexity was initially introduced in the holographic framework [1]. In this framework, it was observed that the conformal field theory (CFT) reaches thermal equilibrium relatively quickly, while the corresponding bulk gravity (wormhole) takes a much longer time to reach the same state. To address this issue, Refs. [2, 3] introduced the concept of computational complexity within the holographic framework. This concept suggests that while the emergence of spacetime is related to quantum entanglement, the evolution of space occurs through computational complexity.

The concept of complexity has become increasingly essential in high-energy physics even without the holographic principle. First, the so-called computational complexity describes the minimum number of logical steps required for a task [4]. Furthermore, the method of calculating the complexity was first proposed by Nielson, *e.t.c*, dubbed as the geometrical method [5–7]. Another approach is highly related to the "Fubini study" distance of the geometry of information [8]. These two geometrical methods are highly dependent on the choice of the geometry of the parametric manifold. For more precisely capturing the information for the quantum state itself, the concept of Krylov complexity was proposed using the Lanczos algorithm [9], which is explicitly related to the quantum state without needing the parametric manifold. Since this method is free of ambiguities compared with the previous two ones, there will be similarities and differences between them. According to the concept of Krylov complexity, the universal operator growth was proposed [10]. Once the precise quantum state is given, we could analyze its Krylov complexity, Krylov entropy, and Lanczos coefficient based on the Lanczos algorithm [9]. For the connection between the Krylov complexity and the circuit complexity, Ref. [11] has shown that they cannot be compatible with each other. However, Ref. [12] demonstrated that the Krylov complexity was proportional to the distance of the "Fubini-Study" metric.

Recently, the Krylov complexity has been broadly applied to condensed matter and high-energy physics. Ref. [13] has systematically analyzed the Krylov complexity in various polynomials dubbed as the orthogonal basis. Due to the importance of the SKY model in high energy physics, the Krylov complexity can also be implemented into this field [14–16]. Meanwhile, the Krylov complexity can be applied to the generalized coherent state [17], Ising and Heisenberg models [18–20], conformal field theory [21, 22], topological phases of matter [23] and even extend into the quantum field theory [24, 25]. Ref. [26] proved that the chaos can be understood as a delocalization in Krylov complexity. Furthermore, one could observe the exponential growth of Krylov complexity in integrable systems with saddle-dominated scrambling, whose universal features can be verified by [28]. More recent developments of Krylov complexity can be found in Refs. [29–46]. Especially, the concept of Krylov complexity can be extended into various fields [47].

We aim to investigate the Krylov complexity for the whole early universe, including the inflationary period, radiation-dominated period (RD), and matter-domination period (MD). Some research has examined the computational complexity for inflation [48–52], where the analysis demonstrated that there is oscillation at the very beginning of inflation, and the evolution was similar in post inflation period. Once considering the quantum effects via various quantum frameworks, the complexity will show the irregular oscillation during inflation providing a new method for distinguishing various inflationary models [55]. Quite a few researches are investigating the Krylov complexity in the early universe. Ref. [56] is the first one who investigate Krylov complexity in inflation by evaluating the values of non-trivial sound speed, where their method is based on the closed system's method. However, our universe is an open system. In light of the open system's method, Ref. [57] investigated the Krylov complexity within the framework of modified dispersion relation in inflation, indicating that the inflation behaves as a strong dissipative system and the overall trend of Krylov complexity is increasing. The key ingredient for exploring the

Krylov complexity with the open system's method is constructing the wave function in light of Ref. [58], whose wave function wave from [57] will serve as our starting point in this work.

In previous studies, Krylov complexity was applied to the early universe using the thermal state. Refs [59, 60] examined Krylov complexity by considering the contribution of the potential (quadratic term) and the violation of slow-roll conditions. The potential was approximated to be the quadratic term around the minimum in our previous work [59], which may not capture fully precise information. In the upcoming work, we plan to include more models such as the Higgs potential [61], the potential of Starobinsky inflation (R^2 inflation) [62], and the potential of chaotic inflation [63]. These models can cover most inflationary models, especially those favored by current observations, which indicate that the potential shape is a plateau. It has been suggested by Ref. [64] that many inflationary models can be unified into the so-called α attractors, whose potential is similar to R^2 inflationary potential. Additionally, Ref. [65] demonstrated a relation between the Bunch-Davies vacuum and the two-mode squeezed state. We will continue to use the two-mode squeezed state to investigate the Krylov complexity for the entire early universe in light of these two factors.

This paper will be organized as follows. In Sec. 2, we will introduce the Lanczos algorithm. Sec. 3 will give a brief introduction to the early universe, including inflation, RD, and MD, and three different kinds of potentials. Sec. 4 will give the two-mode squeezed state, and the numerical solutions of r_k in different periods. Sec. 5 will investigate the Krylov complexity in a method of closed system. Sec. 5.2 will investigate the Krylov entropy in a method of closed system. Sec. 6 will give the Lanczos coefficient and Krylov complexity with the approach of open system, where we are the first to derive the evolution equation of ϕ_k and r_k based on the open two-mode squeezed state. Finally, the conclusion and outlook will be given in Sec. 7.

2 Lanczos algorithm with the approach of closed system

In this section, we will mainly introduce the Lanczos algorithm with the approach of closed system. First, the operator $\mathcal{O}(t)$ in Heisenberg picture needs to be defined as follows,

$$\partial_t \mathcal{O}(t) = i[H, \mathcal{O}(t)] \quad (2.1)$$

where H is the Hamilton and its solution is

$$\mathcal{O}(t) = e^{iHt} \mathcal{O} e^{-iHt} \quad (2.2)$$

Next, let's define the Liouvillian super-operator \mathcal{L}_X as $\mathcal{L}_X Y = [X, Y]$, where $[,]$ denotes the commutator. We apply this to Eq. (2.2), the operator can also be expressed as

$$\mathcal{O}(t) = e^{i\mathcal{L}t} \mathcal{O} = \sum_{n=0}^{\infty} \frac{(it)^n}{n!} \mathcal{L}^n \mathcal{O}(0) = \sum_{n=0}^{\infty} \frac{(it)^n}{n!} \tilde{\mathcal{O}}_n \quad (2.3)$$

where $\mathcal{L}^n \mathcal{O} = \tilde{\mathcal{O}}_n = [H, \tilde{\mathcal{O}}_{n-1}]$ which can serve as the basis for the Hilbert space.

$$\mathcal{O} \equiv |\tilde{\mathcal{O}}\rangle, \mathcal{L}^1 \mathcal{O} \equiv |\tilde{\mathcal{O}}_1\rangle, \mathcal{L}^2 \mathcal{O} \equiv |\tilde{\mathcal{O}}_2\rangle, \mathcal{L}^3 \mathcal{O} \equiv |\tilde{\mathcal{O}}_3\rangle \dots \quad (2.4)$$

However, there are not orthogonal bases. In order to construct an orthogonal basis, we use the Lanczos algorithm. The first two operators become

$$\mathcal{O}_0 = |\tilde{\mathcal{O}}_0) = \mathcal{O}, \quad |\mathcal{O}_1) = b_1^{-1} \mathcal{L}|\mathcal{O}_0) \quad (2.5)$$

where $b_1 = \sqrt{(\tilde{\mathcal{O}}_0 \mathcal{L} | \mathcal{L} \tilde{\mathcal{O}}_0)}$ describing the normalized vector. And the next orthogonal basis can be written by

$$|\mathcal{O}_n) = b_n^{-1} |A_n) \quad (2.6)$$

with

$$|A_n) = \mathcal{L}|\mathcal{O}_{n-1}) - b_{n-1}|\mathcal{O}_{n-2}), \quad b_n = \sqrt{(A_n | A_n)} \quad (2.7)$$

where b_n represents the Lanczos coefficients. This iterative relation will stop and produce the finite orthogonal Krylov basis if $b_n = 0$. Subsequently, we can express Eq. (2.3) as follows,

$$\mathcal{O}(t) = e^{i\mathcal{L}t} \mathcal{O} = \sum_{n=0}^{\infty} (i)^n \phi_n(t) |\mathcal{O}_n) \quad (2.8)$$

where ϕ_n is the wave function satisfying with $\sum_n |\phi_n|^2 = 1$. By substituting Eq. (2.8) into the Schrödinger equation, we can obtain

$$\partial_t \phi_n(t) = b_n \phi_{n-1} - b_{n-1} \phi_{n+1} \quad (2.9)$$

Next, we can define the Krylov complexity using the wave function ϕ_n as follows

$$K = \sum_n n |\phi_n|^2 \quad (2.10)$$

Additionally, the Lanczos coefficient can be bounded via [10],

$$b_n \leq \alpha n + \eta \quad (2.11)$$

where α and η encodes different information in various models. It should be noticed that $b_n = \alpha n + \eta$, meaning that the system is a maximal chaotic dynamical system. For the case of maximal chaos, we could build the relation between the Lyapunov index and γ and α as follows,

$$\lambda = 2\alpha \quad (2.12)$$

In this work, we will investigate the Krylov complexity for the entire early universe, thus the formula of scale factor $a(\eta)$ should be introduced.

3 Some setup of early universe

In this section, we will first give some basis of scale factor in distinctive periods. Following the notation of our previous work [59], one of the core goal of this work is examining the impact of inflationary potential for the Krylov complexity in RD and MD due to the violation of slow-roll conditions. The Mukhannov-Sasaki variable contains the contribution of potential which cannot show the explicit contribution to the Krylov complexity. That is why we just perturb the inflaton field explicitly in this paper. Thereafter, we will give some very important inflationary potentials, namely, the chaotic inflationary potential, Starobinsky's inflationary potential (R^2 inflation) and Higgs potential.

3.1 Inflation, RD and MD

We will follow the notation of [66] to introduce the scale factor. The background metric is the Friedman-Lemaitre-Robertson-Walker metric,

$$ds^2 = a^2(\eta)(-d\eta^2 + d\vec{x}^2), \quad (3.1)$$

where $a(\eta)$ is the scale factor. Here, we will assume a single component universe, which means that the universe will experience the inflation, RD and MD, respectively. We could use equation of state to characterize the universe via

$$w_I = \frac{P_I}{\rho_I}, \quad (3.2)$$

where P_I and ρ_I is the pressure and energy density of the corresponding periods parameterized by I . For obtaining the relation between the conformal time and the scale factor, we need the comoving distance,

$$\chi_{ph}(\eta) = \int_{t_i}^t \frac{dt}{a} = \int_{\ln a_i}^{\ln a} (aH)^{-1} d \ln a \quad (3.3)$$

where $\chi_{ph}(\eta)$ is the comoving distance in the event horizon of particle. In light of w_I , the Hubble radius can be replaced by

$$(aH)^{-1} = H_0^{-1} a^{\frac{1}{2}(1+3\omega)} \quad (3.4)$$

where we use ω to take place of ω_I for simplify. Integrating equation (3.3) yields the relation between the scale factor and the conformal time

$$\eta = \frac{2H_0^{-1}}{(1+3\omega)} a^{\frac{1}{2}(1+3\omega)} \quad (3.5)$$

Consequently, we can derive the relation for various time periods

$$\eta = \begin{cases} -(aH_0)^{-1}, & (\omega = -1), \text{ inflation} \\ aH_0^{-1}, & (\omega = \frac{1}{3}), \text{ RD} \\ 2\sqrt{a}H_0^{-1}, & (\omega = 0), \text{ MD} \end{cases} \quad (3.6)$$

One could see that the various values of ω describe the distinctive periods.

In the following text, we will discuss the fundamental basis for the different periods in the evolution of the universe. Initially, the universe is created by a singularity, followed by a period of exponential expansion known as inflation. During this phase, the curvature perturbation transitions from the quantum level to the classical level after the horizon exits, leaving an imprint on the Cosmic Microwave Background (CMB). Subsequently, the universe enters the Radiation Dominated (RD) era, characterized by an energy density given by the equation $\rho_{\text{rad}}(t) = \rho_{\text{rad}0} \frac{a_0^4}{a(t)^4}$, where $\rho_{\text{rad}0}$ and a_0 represent the initial values of the energy density and the scale factor of RD. During the RD era, particles are relativistic, but as the temperature decreases, they become increasingly non-relativistic. This leads

the universe into the matter-dominated (MD) epoch, where the energy density is given by $\rho_{\text{mat}_0}(t) = \rho_{\text{mat}_0} \frac{a_0^3}{a(t)^3}$. The transition from the RD to the MD epoch occurs when the energy density of radiation becomes equal to the energy density of matter. Once entering MD, there is a process called preheating where the particles will be generated via this process. First, we give the full action for the single field inflation,

$$S = \int d\eta d^3 \vec{x} \sqrt{-g} \left[\frac{1}{2} g^{\mu\nu} \partial_\mu \phi \partial_\nu \phi - V(\phi) \right], \quad (3.7)$$

where $V(\phi)$ is the potential of inflation. Following the method of [67, 68], the equation of motion for background $\phi(t)$ in RD and MD is

$$\ddot{\phi}(t) + 3H\dot{\phi}(t) + V(\phi)_{,\phi} = 0, \quad (3.8)$$

where $\ddot{\phi}(t) = \partial_t^2 \phi(t)$ and the similar work can be found in our previous works [77, 78]. Defining with the effective mass $m_{\text{eff}} = \frac{d^2 V}{d\phi^2}$ and changing variable as $\tilde{\phi}(t) = a^{3/2} \phi(t)$, Eq. (3.8) will become

$$\ddot{\tilde{\phi}}(t) + m_{\text{eff}}^2 \tilde{\phi}(t) = 0, \quad (3.9)$$

the solution of Eq. (3.9) is $\phi(t) = a^{-3/2} \cos(m_{\text{eff}} t)$ where it is the solution of $\phi(t)$ in preheating period and we have neglected the term of $\frac{9}{4} H^2 \tilde{\phi} + \frac{3}{2} \dot{H} \tilde{\phi}$ since it is much smaller compared with potential. It should be noticed that the solution is in terms of physical time t . In this paper, we will use $d\eta = \frac{dt}{a}$ to transform into the conformal time for the latter investigations, which is denoted by Eq. (3.6).

3.2 Various inflationary potentials

There are lots of inflationary models that represent distinctive inflationary potentials. Current observations favor the concave potentials [71], where the potential of R^2 inflation belongs to this potential. Additionally, the R^2 inflation agrees with the observations from inflation to large scales. From the theoretical aspect, we could see that many inflationary models can be unified into the so-called α attractors inflationary models [64], where the other models and R^2 inflationary model belong to the same kind of inflationary models. Being armed with these two reasons, we will introduce R^2 inflation. According to the current standard model, the Higgs field is the only scalar field in nature. Therefore, the Higgs potential is our other option [61]. The final choice is the chaotic inflation whose potential is the quadratic term [63]. Finally, we could see that our choices could cover the most inflationary models.

Here, we list the formulas of distinctive inflationary potentials as follows,

$$\begin{cases} V_1 = \frac{1}{2} m^2 \phi^2, \\ V_2 = \frac{3}{4} M^2 M_p^2 (1 - e^{-\sqrt{\frac{2}{3}} \frac{\phi}{M_p}})^2, \\ V_3 = \frac{1}{2} m^2 \phi^2 + \frac{1}{4} \lambda \phi^4, \end{cases} \quad (3.10)$$

where $M_p = (8\pi G)^{-\frac{1}{2}}$ is the definition of the reduced Planck mass. Additionally, M represents the energy scale, and its value can be determined based on the amplitude of the

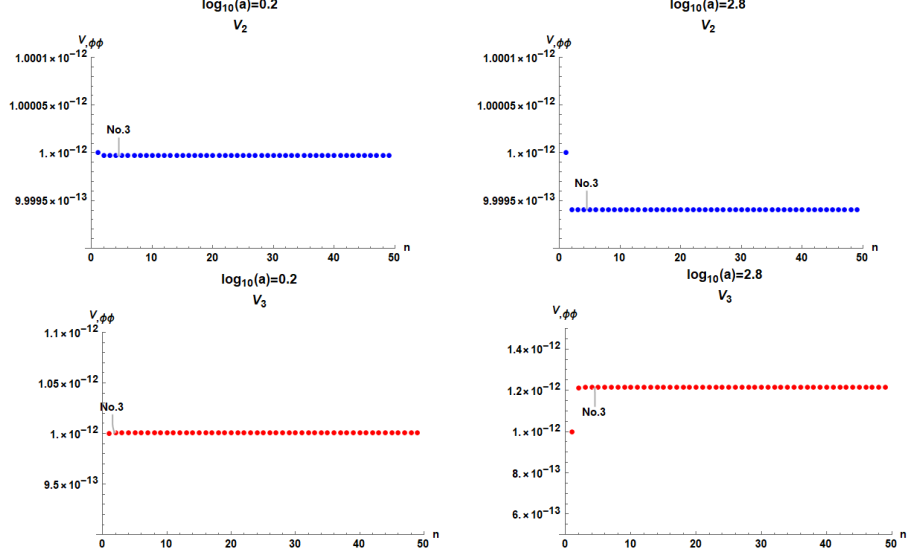


Figure 1. The numeric of $V_{,\phi\phi}$ at first 50 iterations of potential V_2 and V_3 in $\log_{10} a = 0.2$ and $\log_{10} a = 2.8$, in which we set $M_p = 1$, $m = 10^{-6}$; $M^2 = 10^{-12}$ at V_2 , and $\lambda A^2 = 10^{-4}$ at V_3 .

observed power spectrum for primordial perturbations. Being armed with the solution of Eq. (3.8) and $dt = ad\eta$, we could rewrite $V_{\phi\phi}$ as

$$\left\{ \begin{array}{l} V_{1,\phi\phi} = m^2, \\ V_{2,\phi\phi} = M^2 \left(-e^{-\sqrt{\frac{2}{3}} \frac{Aa^{-\frac{3}{2}} \sin(m_{\text{eff}} a \eta)}{M_p}} + 2e^{-2\sqrt{\frac{2}{3}} \frac{Aa^{-\frac{3}{2}} \sin(m_{\text{eff}} a \eta)}{M_p}} \right), \\ V_{3,\phi\phi} = m^2 + 3\lambda A^2 a^{-3} \sin^2(m_{\text{eff}} a \eta) \end{array} \right. \quad (3.11)$$

where $\phi(t) = Aa^{-\frac{3}{2}} \sin(m_{\text{eff}} t)$. For the effective mass m_{eff} , we have $m_{\text{eff}}^2 = \frac{d^2 V(x)}{dx^2}$, and it is evident that $m_{\text{eff}} = \sqrt{V_{i,\phi\phi}}$ in our work ($i = 1, 2, 3$). According to effective mass for the distinctive inflationary models, we need the iterations for V_2 and V_3 in terms of $\log_{10} a$ followed by [57]. To determine whether the functions V_2 and V_3 converge within the defined interval, we performed iterations at multiple sampling points ranging from $\log_{10} a = 0$ to $\log_{10} a = 6$ with the step 0.05. Our findings reveal that all points ranging from $\log_{10} a = 0$ to $\log_{10} a = 6$ are all convergent. As an illustration, Fig. 1 clearly shows the iterations for potential V_2 and V_3 , where we have performed 50 times iterations for two specific values of $\log_{10} a$. Let us mention the range of parameters as shown in Fig. 1, the potential can be constraint by the COBE normalization [72], whose values are bounded below 10^{-10} in Planck units, and the inflationary field is a large field and its maximal value is around 100. Consequently, the effective mass for various potentials is around 10^{-6} and other parameters are set according to this logic.

Fig. 2 depicts the evolution of $V_{,\phi\phi}$ with respect to $\log_{10} a$ in RD and MD, using the third iteration of V_2 and V_3 via Fig. 1. The evolution of inflation is neglected due to the violation of slow-roll conditions. From Fig. 2, we could see that the effective mass of R^2 inflation will decrease in RD and then it will grow to the constant (10^{-12}) with the

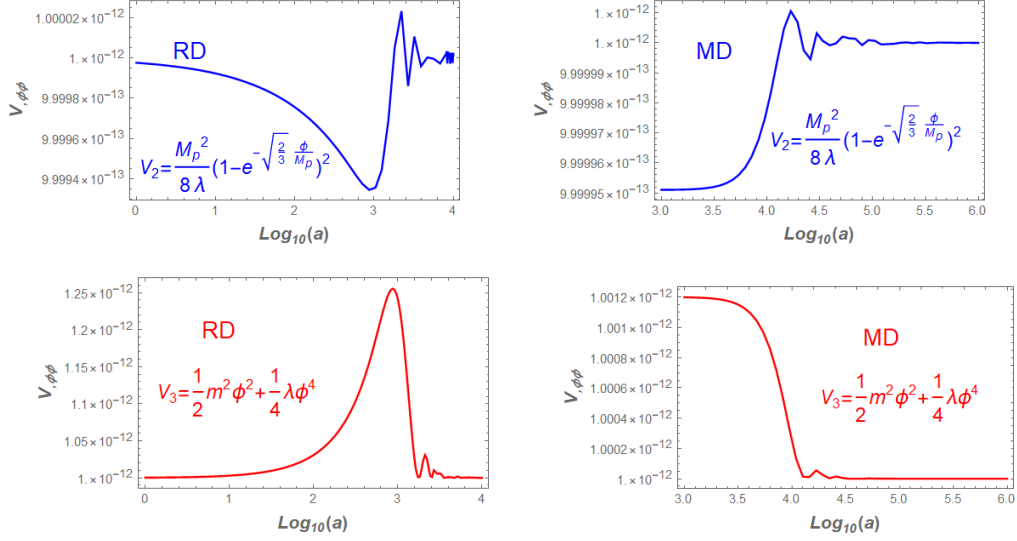


Figure 2. The numeric of $V_{,\phi\phi}$ in terms of $\log_{10} a$ for potential V_2 , and V_3 in RD and MD, in which we replace its exact value with the third iteration of V_2 and V_3 . We set $\theta_0 = 0$, $M_p = 1$, $m = 10^{-6}$; $M^2 = 10^{-12}$ at V_2 , and $\lambda A^2 = 10^{-4}$ at V_3 .

oscillations. For the potential of the Higgs field, it is different which shows that there is a peak in RD and after that, it will decrease into some constants. But, it indicates that the effective mass of V_2 and V_2 are of almost the same order based on the COBE normalization [72].

In this section, we provide an introduction to inflation, RD, and MD, which are characterized by the corresponding scale factor. We then present three essential inflationary potentials that encompass most types of inflationary models. Additionally, we provide an overview of preheating, during which the background of the inflaton field oscillates around the minimum. Subsequently, we incorporate the background solution for the inflaton into the numerical calculation of the effective mass for these three distinct potentials.

4 Evolution of two-mode squeezed state

In this section, we will follow the method of [57] for investigating the evolution of r_k and ϕ_k in inflation, RD and MD. We have evaluated the quantum circuit complexity in various inflationary frameworks [53–55].

4.1 Two-mode squeezed state

For obtaining the two-mode squeezed state, we should introduce the unitary operator as follows,

$$\mathcal{U}_k = \hat{\mathcal{S}}_k(\phi_k, r_k) \hat{\mathcal{R}}_k(\theta_k) \quad (4.1)$$

with

$$\hat{\mathcal{S}}_k = \exp \left[r_k(\eta) \left(e^{-2i\phi_k(\eta)} \hat{c}_{\vec{k}} \hat{c}_{-\vec{k}} - e^{2i\phi_k(\eta)} \hat{c}_{-\vec{k}}^\dagger \hat{c}_{\vec{k}}^\dagger \right) \right] \quad (4.2)$$

$$\hat{\mathcal{R}}_k(\theta_k) = \exp \left[-i\theta_k(\eta)(\hat{c}_{\vec{k}}\hat{c}_{\vec{k}}^\dagger + \hat{c}_{-\vec{k}}^\dagger\hat{c}_{-\vec{k}}) \right] \quad (4.3)$$

where $\hat{\mathcal{S}}_k$ is the squeezed parameter and $\hat{\mathcal{R}}_k(\theta_k)$ is the rotation parameter that will be neglected since it only contributes the phase factor of wave function. Then, by applying $\hat{\mathcal{S}}_{\vec{k}}(r_k, \phi_k)$ to the vacuum state, we can express the wave function of the two-mode squeezed state as follows

$$|\psi\rangle = \hat{\mathcal{S}}_{\vec{k}}(r_k, \phi_k)|0;0\rangle_{\vec{k},-\vec{k}} = \frac{1}{\cosh r_k} \sum_{n=0}^{\infty} (-1)^n e^{2in\phi_k} \tanh^n r_k |n;n\rangle_{\vec{k},-\vec{k}}. \quad (4.4)$$

Being armed with this wave function, we could proceed the numeric of ϕ_k and r_k . But the evolution of ϕ_k and r_k is based on the total action (3.7).

4.2 The evolution of $r_k(\eta)$ and $\phi_k(\eta)$

In this work, we will evaluate the impact of potential for the Krylov complexity, where the Mukhanov-Sasaki variable contains the contribution of potential. Consequently, we cannot observe the explicit influence from potential. Therefore, we will directly perturb the total action into the second order,

$$S = \frac{1}{2} \int d\eta d^3x \left[f'^2 - (\partial_i f)^2 + \left(\frac{a'}{a}\right)^2 f^2 - 2f' f \frac{a'}{a} - a^2 V_{,\phi\phi} f^2 \right] \quad (4.5)$$

where $f(\eta, \vec{x})$ is the perturbation of inflaton defined by $\phi(\eta, \vec{x}) = \bar{\phi}(\eta) + \frac{f(\eta, \vec{x})}{a(\eta)}$. For the slow-roll condition in inflation, we could neglect the potential, namely $\left(\frac{a'}{a}\right)^2 f^2 - 2f' f \frac{a'}{a} \gg a^2 V_{,\phi\phi} f^2$. Then, we could construct the Hamilton via $H = \int d^3x d\eta (\pi f' - \mathcal{L})$ where \mathcal{L} represents the Lagrangian and π is the so-called conjugate momentum defined by

$$\pi(\eta, \vec{x}) = \frac{\delta L}{\delta f'(\eta, \vec{x})} = f' - \frac{a'}{a} f. \quad (4.6)$$

According to Eq. (4.5) and Eq. (4.6), we could obtain

$$H = \frac{1}{2} \int d^3\eta [\pi^2 + (\partial_i f)^2 + \frac{a'}{a}(\pi f + f\pi) + a^2 V_{,\phi\phi} f^2]. \quad (4.7)$$

Using the Fourier decomposition of operator $\hat{f}(\eta, \vec{x})$ and $\hat{\pi}(\eta, \vec{x})$,

$$\hat{f}(\eta, \vec{x}) = \int \frac{d^3k}{(2\pi)^{3/2}} \sqrt{\frac{1}{2k}} (\hat{c}_{\vec{k}}^\dagger f_{\vec{k}}^*(\eta) e^{-i\vec{k}\cdot\vec{x}} + \hat{c}_{\vec{k}} f_{\vec{k}} e^{i\vec{k}\cdot\vec{x}}), \quad (4.8)$$

$$\hat{\pi}(\eta, \vec{x}) = i \int \frac{d^3k}{(2\pi)^{3/2}} \sqrt{\frac{k}{2}} (\hat{c}_{\vec{k}}^\dagger u_{\vec{k}}^*(\eta) e^{-i\vec{k}\cdot\vec{x}} - \hat{c}_{\vec{k}} u_{\vec{k}} e^{i\vec{k}\cdot\vec{x}}). \quad (4.9)$$

Substituting equations (4.8) and (4.9) into equation (4.7) to obtain the Hamiltonian operator,

$$\hat{H}_k = \left(k + \frac{a^2 V_{,\phi\phi}}{2k}\right) (\hat{c}_{\vec{k}}\hat{c}_{\vec{k}}^\dagger + \hat{c}_{-\vec{k}}^\dagger\hat{c}_{-\vec{k}}) + \left(\frac{a^2 V_{,\phi\phi}}{2k} + i\frac{a'}{a}\right) \hat{c}_{-\vec{k}}^\dagger\hat{c}_{\vec{k}}^\dagger + \left(\frac{a^2 V_{,\phi\phi}}{2k} - i\frac{a'}{a}\right) \hat{c}_{-\vec{k}}\hat{c}_{\vec{k}}. \quad (4.10)$$

Being armed with Hamiltonian operator and Schrödinger equation

$$i \frac{d}{d\eta} |\psi\rangle = \hat{H}_k |\psi\rangle, \quad (4.11)$$

we could obtain the evolution of equation of r_k and ϕ_k

$$\begin{aligned} r'_k &= \frac{a^2 V_{,\phi\phi}}{2k} \sin 2\phi_k - \frac{a'}{a} \cos 2\phi_k, \\ \phi'_k &= -k - \frac{a^2 V_{,\phi\phi}}{2k} + \left(\frac{a'}{a} \sin 2\phi_k + \frac{a^2 V_{,\phi\phi}}{2k} \cos 2\phi_k \right) \coth 2r_k. \end{aligned} \quad (4.12)$$

In inflation, Eq. (4.12) will nicely recover into the case of

$$\begin{aligned} r'_k &= -\frac{a'}{a} \cos(2\phi_k), \\ \phi'_k &= -k + \frac{a'}{a} \sin(2\phi_k) \coth(2r_k). \end{aligned} \quad (4.13)$$

It is very difficult to obtain the numeric of Eq. (4.12), thus we could make a variable transformation, $y = \log_{10} a$, to numerically solve Eq. (4.12),

$$\begin{aligned} \frac{dr_k}{dy} &= \frac{\ln(10) 10^{\frac{y}{2}(5+3\omega)} V_{,\phi\phi}}{2k H_0} \sin 2\phi_k - \ln(10) \cos 2\phi_k \\ \frac{d\phi_k}{dy} &= -\frac{\ln(10) 10^{\frac{y}{2}(1+3\omega)} k}{H_0} - \frac{\ln(10) 10^{\frac{y}{2}(5+3\omega)} V_{,\phi\phi}}{2k H_0} + \left(\ln(10) \sin 2\phi_k \right. \\ &\quad \left. + \frac{\ln(10) 10^{\frac{y}{2}(5+3\omega)} V_{,\phi\phi}}{2k H_0} \cos 2\phi_k \right) \coth 2r_k \end{aligned} \quad (4.14)$$

where we have utilized Eq. (3.5) and $\frac{a'}{a} = H_0 a^{-\frac{1}{2}(1+3\omega)}$.

Before analyzing the figure of r_k , it's important to note that the Krylov complexity depends only on r_k . Therefore, we only provide the numerical values of r_k in Fig. 3 based on Eq. (4.14). In this equation, we have set $H_0 = 1$ for simplicity and used various values of k in different time periods. The first panel of Fig. 3 illustrates the evolution of r_k during inflation. There is an oscillation before the horizon exits, and then r_k will grow linearly, consistent with the standard case of [57]. As we transition to the radiation-dominated era (RD), we observe that r_k will increase to some constant value that oscillates around this value. Interestingly, different potentials produce almost the same trend for r_k , indicating that the specific potential does not significantly impact the evolution of r_k . This observation also applies to the matter-dominated era (MD), where the evolution trend is similar to RD. However, we notice that varying momentum significantly affects r_k , leading to oscillations as the value of k decreases. Although we cannot distinguish between the various potentials using Fig. 3, our numerical data still demonstrates that the evolution of r_k is significantly different whether there is a potential or not. It's worth noting that we cannot provide the values of r_k without a potential, as this is not physically meaningful. The potential cannot be ignored due to the violation of slow-roll conditions.

In this section, we have analyzed the evolution of r_k for different inflationary potentials within a single-field inflationary framework. Our research indicates that the value of r_k

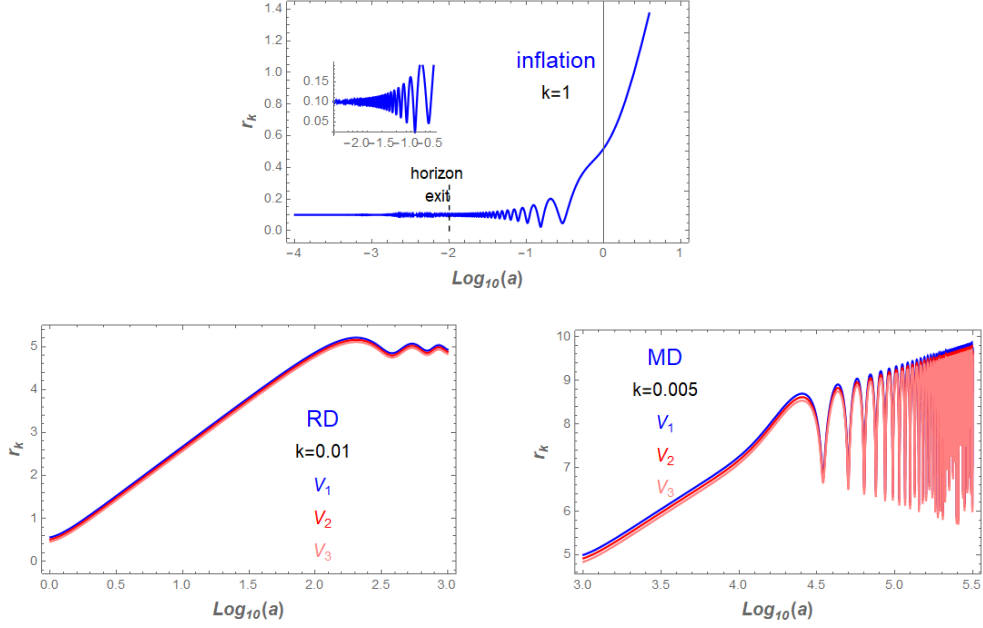


Figure 3. The numerical solution of R_k in terms of $\log_{10} a$ for three different periods (inflation, RD, and MD), where we set $H_0 = 1$. $k = 1$ at period inflation, $k = 0.01$ at period RD, $k = 0.005$ at period MD for simplicity.. The effect of potential is always ignored in slow-roll inflation. But in RD and MD periods, the influence can be seen by using different potential energies as shown in these panels.

increases during inflation. The behavior of r_k in radiation-dominated (RD) and matter-dominated (MD) eras is similar and will oscillate around constant values. Our numerical analysis also shows that various inflationary models produce a similar trend for r_k . Additionally, we have observed that the scale factor and momentum have a significant impact on the evolution of r_k . All of the details are encoded in Fig. 3.

5 Krylov complexity in closed system

In this section, we will investigate the Krylov complexity in the method of closed system [53–55], consisting of the Krylov complexity and Krylov entropy.

5.1 Krylov complexity

For obtaining the Krylov complexity, the most essential quantity is the wave function. First, the two-mode squeezed state wave function can be represented by Krylov basis as follows,

$$\mathcal{O}(t) = \sum_{n=0}^{\infty} (i)^n \phi_n(t) |\mathcal{O}_n\rangle = \frac{1}{\cosh r_k} \sum_{n=0}^{\infty} (-1)^n e^{2in\phi_k} \tanh^n r_k |n; n\rangle_{\vec{k}, -\vec{k}}. \quad (5.1)$$

Then, we could find the explicit wave function ϕ_n

$$\phi_n = \frac{1}{\cosh r_k} (-e^{2i\phi_k} \tanh r_k)^n. \quad (5.2)$$

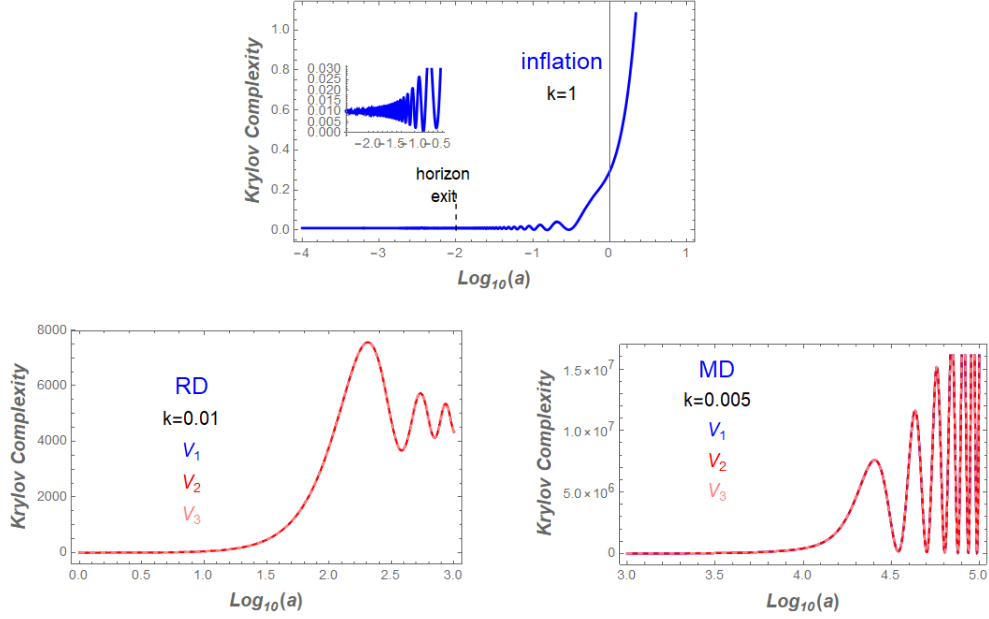


Figure 4. The numerical of Krylov complexity in terms of $\log_{10} a$ for three different periods (inflation, RD, and MD), where we set $H_0 = 1$. $k = 1$ at period inflation, $k = 0.01$ at period RD, $k = 0.005$ at period MD for simplicity.

We can define the Krylov complexity in terms of ϕ_n

$$K = \sum_n n |\phi_n|^2 = \cosh^2 r_k \tanh^2 r_k = \sinh^2 r_k. \quad (5.3)$$

It is explicitly showing that the Krylov complexity is independent of ϕ_k , that is why we only list the figure of r_k .

Being armed with Eq. (5.3), we could give its numeric in Fig. 4, indicating the evolution of Krylov complexity in inflation, RD, and MD. Fig. 4 clearly shows that the Krylov complexity is enhanced in inflation which is consistent with the standard case of the modified dispersion within the framework [57]. Similar work investigated the Krylov complexity for the exponential expansion for de-Sitter spacetime corresponding to the inflation [56]. Ref. [56] mentioned that the Krylov complexity equals the average particle number proportional to the volume. Thus we could see that this simple analysis is consistent with the CV conjuncture [1], in which the complexity is equaled to the volume of wormhole under the framework of holography. However, the method of [56] is for the closed system.

In the case of RD and MD, it is observed that the Krylov complexity will increase to certain constant values that fluctuate around this value. Additionally, different patterns of inflationary models tend to produce similar trends of Krylov complexity in different periods. Our analysis aligns with the findings of [73], where the Krylov complexity will saturate some constant values even after the scrambling time in a closed system. The scrambling time will be assessed in the context of an open system, particularly with regard to the Lanczos coefficient, Lyapunov index, *e.t.c.*

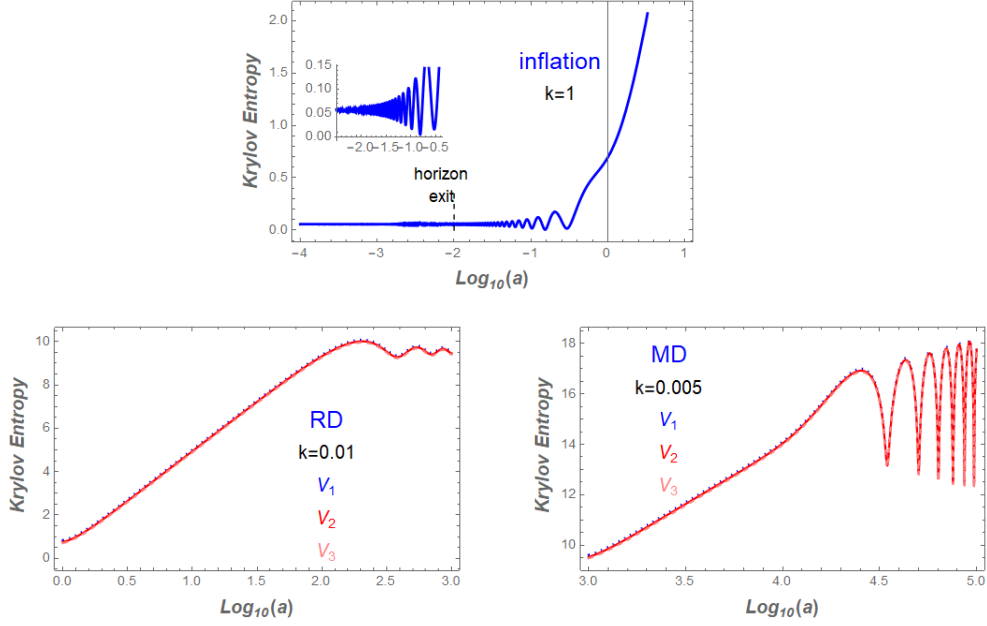


Figure 5. The numerical of Krylov entropy in terms of $\log_{10} a$ for three different periods (inflation, RD, and MD), where we set $H_0 = 1$. $k = 1$ at period inflation, $k = 0.01$ at period RD, $k = 0.005$ at period MD for simplicity.

5.2 Krylov Entropy

In a quantum system, entropy is defined as a measure of the disorder of a system. The Krylov entropy (K-entropy) can be used to test the level of disorder of curvature perturbation. Following [73], the K-entropy has the following form

$$\begin{aligned}
 S_K &= - \sum_{n=0}^{\infty} |\phi_n|^2 \ln |\phi_n|^2 \\
 &= \cosh^2 r_k \ln(\cosh^2 r_k) - \sinh^2 r_k \ln(\sinh^2 r_k)
 \end{aligned}
 \tag{5.4}$$

where ϕ_n is the wave function (4.4). Once given the analytic formula of K-entropy, we could numerically simulate it in various epochs as shown in Fig. 5.

Fig. 5 indicates a complete evolution of K-entropy in inflation, RD and MD, which is similar to Krylov complexity. We could see that the curvature of perturbation will be more and more disorder in inflation. For RD and MD, the disorder will be enhancing and then saturates to some constant values and the total trend is enhancing, where the trend is also highly related the scale factor. From another aspect, the preheating will generate the particles occurred at MD that leads to the growth of K-entropy.

Let's discuss Section 5. In this section, we provide a comprehensive analysis of Krylov complexity throughout the early universe. Our numerical data clearly indicates that different potentials yield almost identical patterns of Krylov complexity and K-entropy. Specifically, Krylov complexity increases during inflation and then stabilizes at constant values during RD and MD. This same behavior is observed for K-entropy. Additionally, we must

examine the Lanczos coefficient (equivalent to the Lyapunov index in maximal chaos), which remains consistent in both the closed and open system methods.

6 Krylov complexity with the approach of open system

The preheating process in MD and RD is a highly non-equilibrium process that creates particles [67, 68]. In addition, Ref. [74] demonstrated that the universe's evolution breaks the time invariance when the temporal direction is reversed, leading to a violation of energy conservation. Due to these reasons, the open system approach is considered to be more realistic compared to the closed system method. We will follow the method of [58] to investigate the Krylov complexity.

6.1 Lanczos coefficient and dissipation coefficient

Firstly, the general operator in Heisenberg's picture has the following form,

$$\mathcal{O}(\eta) = e^{i\mathcal{L}_o\eta} \quad (6.1)$$

where the Lindbladian \mathcal{L}_o , also known as the Hamiltonian, acts on the Krylov basis, we can obtain

$$\mathcal{L}_o|\mathcal{O}_n\rangle = -ic_n|\mathcal{O}_n\rangle + b_{n+1}|\mathcal{O}_{n+1}\rangle + b_n|\mathcal{O}_{n-1}\rangle \quad (6.2)$$

where c_n encodes the information of the open system and b_n is the Lanczos coefficient. Due to this extra term, we could divide the total Hamiltonian (also known as Lindbladian) into two parts which can be represented by

$$\mathcal{L}_o = \mathcal{H}_k = \mathcal{H}_{close} + \mathcal{H}_{open} \quad (6.3)$$

In our work, \mathcal{L}_o is the Hamiltonian Eq. (4.10). In light of (6.2), we can easily obtain the open part (generating c_n) of Hamiltonian,

$$\mathcal{H}_{open} = (k + \frac{a^2 V_{,\phi\phi}}{2k})(\hat{c}_{-\vec{k}}^\dagger \hat{c}_{-\vec{k}} + \hat{c}_{\vec{k}} \hat{c}_{\vec{k}}^\dagger) \quad (6.4)$$

and the close part (generating b_n and b_{n-1}) is

$$\mathcal{H}_{close} = (\frac{a^2 V_{,\phi\phi}}{2k} + i\frac{a'}{a})\hat{c}_{\vec{k}}^\dagger \hat{c}_{-\vec{k}}^\dagger + (\frac{a^2 V_{,\phi\phi}}{2k} - i\frac{a'}{a})\hat{c}_{\vec{k}} \hat{c}_{-\vec{k}} \quad (6.5)$$

where $|\mathcal{O}_n\rangle = |n_{\vec{k}}; n_{-\vec{k}}\rangle$. By substituting Eq. (6.4) and Eq. (6.5) into Eq. (6.2), we can obtain the equations for c_n and b_n as

$$c_n = i(2n+1)(k + \frac{a^2 V_{,\phi\phi}}{2k}). \quad (6.6)$$

$$b_n = n\sqrt{[(\frac{a^2 V_{,\phi\phi}}{2k})^2 + (\frac{a'}{a})^2]}. \quad (6.7)$$

Here, we will discuss more about b_n and c_n . Ref. [75] has introduced the a_n corresponding to c_n in our work and also stated that c_n is highly related to the dissipative coefficient.

Meanwhile, we could see that b_n is the same for the closed system and open system since it is precisely determined by the Hamiltonian.

In Ref. [10], it has clearly indicated that the dynamical system is an infinite, non-integrable, many-body system as $b_n = \alpha n + \gamma$, where α and γ are two parameters determined by various models. In our case, we could see that $b_n \propto n$, thus the whole early universe is an ideal chaotic system.

6.1.1 b_n , c_n and μ_2

In this paper, we will follow the discussion and the notation via [57]. We first discuss the property of c_n in our paper. Recalling that the Eq. (2.9) (Schrödinger equation essentially) only includes the Lanczos coefficient. The parameter c_n will appear in the following modified equation,

$$\partial_\eta \phi + 2b_n \partial_n \phi + \tilde{c}_n \phi = 0, \quad (6.8)$$

where we have defined $\tilde{c}_n = -ic_n$, meanwhile we have used the $b_{n+1} \approx b_n$ and $\phi_{n+1} - \phi_{n-1} \approx 2\partial_n \phi$ in the continuous limit. b_n and c_n are defined in Eq. (6.6) and Eq. (6.7), respectively. The generic formulas of b_n and c_n are

$$b_n^2 = |1 - \mu_1^2| n(n-1 + \beta), \quad c_n = i\mu_2(2n + \beta) \quad (6.9)$$

where μ_1 , μ_2 and β are determined by various models and μ_2 plays a role of dissipative coefficient as shown in Ref. [57]. In our work, one can explicitly find $\beta = 1$ and combine Eqs. (6.6), (6.7), and (6.9), we find that the parameters μ_1 and μ_2 have the following forms,

$$|1 - \mu_1^2| = \left(\frac{a^2 V_{,\phi\phi}}{2k}\right)^2 + \left(\frac{a'}{a}\right)^2, \quad \mu_2 = k + \frac{a^2 V_{,\phi\phi}}{2k}. \quad (6.10)$$

It should be noticed that μ_2 is mainly determined by k in inflation due to the slow-roll conditions. Once entering RD and MD (taking the contribution of the effective mass into account), we could see that it will be smaller than unity since the effective mass of these three types potentials is much more tiny compared with momentum k . First, we discuss the Lanczos coefficient b_n . Fig. 6 clearly indicates the three distinctive potentials of b_n in inflation, RD and MD, in which the parameters of k , H_0 are set to be the same with the previous plots. As [58] confirmed, the Lyapunov index is equivalent to b_n whose relation is $\lambda = 2\alpha$ with $b_n = \alpha n + \delta$ ($\delta = 0$ in our case), where it is explicitly showing that $\lambda = 2\alpha$, namely $\lambda = b_n$ with $n = 2$ which will be shown in Fig. 6. The physical meaning of λ represents the chaotic feature of dynamical system. Consequently, b_n in our case also manifest the chaotic feature for the early universe.

Figure 6 illustrates the evolution trend b_n in inflation, radiation domination (RD), and matter domination (MD). Based on the discussion regarding b_n , chaos will be heightened due to the exponential expansion of the background space. As the energy decreases, b_n will also decline since the temperature decreases. During MD, particles are generated through a preheating process known as parametric resonance, which leads to an increase in b_n . Finally, we need to analyze the dissipative coefficient μ_2 that is related to c_n , where we

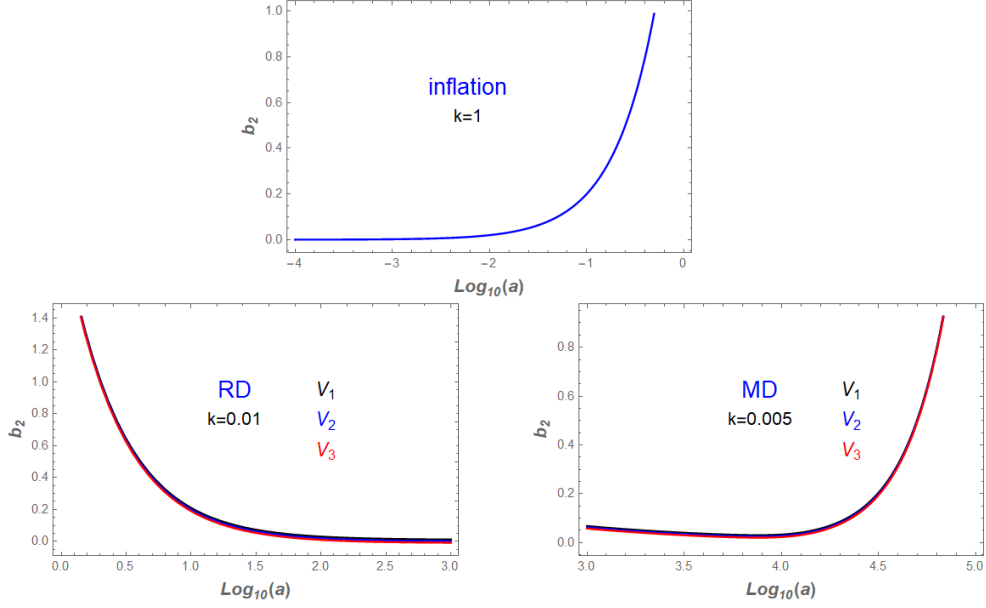


Figure 6. The plot of $b_n = \lambda$ with $n = 2$. The numerical of b_n in terms of $\log_{10} a$ for three different periods (inflation, RD, and MD), where we set $H_0 = 1$. $k = 1$ at period inflation, $k = 0.01$ at period RD, $k = 0.005$ at period MD for simplicity.

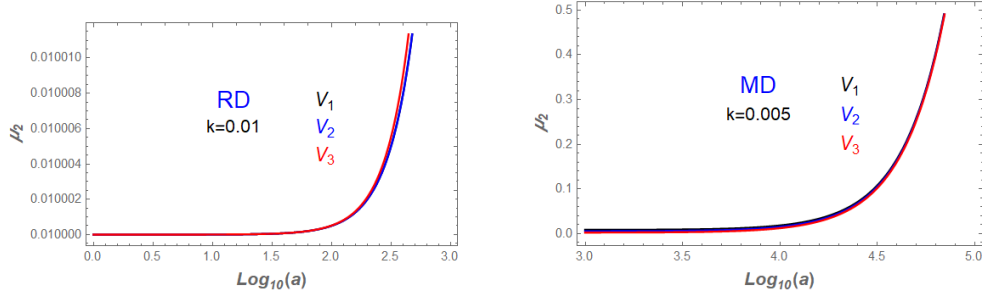


Figure 7. The numerical of dissipative coefficient μ_2 in terms of $\log_{10} a$ for RD and MD, where we set $H_0 = 1$, $k = 0.01$ at period RD, $k = 0.005$ at period MD for simplicity. The value of $m\mu_2$ indicates the RD and MD are weak dissipative systems.

could confirm the previous results via [57]. Fig. 7 clearly shows the evolution in RD and MD. The μ_2 in inflation is not shown in Fig. 7 since $\mu_2 = k = 1$ in light of the values of k for inflation. Ref. [57] claimed that inflation is a strong dissipative system as $\mu_2 \geq 1$, RD and MD are weak dissipative systems as $\mu_2 \ll 1$, which is explicitly confirmed by Fig. 7.

To summarize the chaotic features of the early universe: First, chaos is enhanced by the exponential expansion. Then, as the energy scale diminishes, chaos decreases. Finally, the generation of particles during MD through the preheating process increases chaos once again.

6.2 General discussion of ϕ_n

Before the Krylov complexity, we discuss the general properties of ϕ_n since the definition of Krylov complexity is explicitly represented by $C_K = \sum_{n=1}^{+\infty} n |\phi_n|^2$. We will follow the general discussion of ϕ_n via Refs. [57, 75]. Eq. (6.8) can be rewritten by

$$\partial_\eta \phi + n(\chi\mu\phi + 2\alpha\partial_n\phi) = 0, \quad (6.11)$$

where we have defined $\tilde{c}_n = n\chi\mu$ and $b_n = n\alpha$. As η approaches infinity, the solution of Eq. (6.11) has the form $\phi(n) \propto e^{-n\xi}$ with $\xi = \frac{2\alpha}{\mu\chi}$, where this form will appear in RD or MD due to their weak dissipative nature. In the weak dissipative region, the corresponding Krylov complexity behaves as follows: it increases exponentially at the onset, with the average position given by $C_k \propto e^{2\alpha\eta}$ before reaching η_* . After this point, the Krylov complexity saturates to a constant value ξ when $\eta > \eta_*$, where $\eta_* \sim \frac{1}{2\alpha} \ln \frac{2\alpha}{\chi\mu}$. It is straightforward to demonstrate that $\exp(2\alpha\eta_*) = \xi$. After some simple algebra, we could obtain the formula ξ in our case as follows,

$$\xi = \frac{2\sqrt{\left(\frac{a^2 V_{,\phi\phi}}{2k}\right)^2 + \left(\frac{a'}{a}\right)^2}}{\left(2 + \frac{1}{n}\right)\left(k + \frac{a^2 V_{,\phi\phi}}{2k}\right)} \quad (6.12)$$

From this formula, we can observe that ξ is not strictly constant; it varies with respect to a and k . Consequently, a significant change in the background will have a substantial impact on Krylov complexity. In this section, we examined the general properties of Krylov complexity without providing the precise formula for ϕ_n . To fully capture the information concerning Krylov complexity within the framework of the open system method, it is essential to have the exact wave function for ϕ_n .

6.3 Wave function within the method of open system

Although we constructed the wave function for an open system in reference [57], based on the framework established in [75], our approach is too simplistic to capture the complete information of the open system. Notably, our wave function, as shown in [57], can effectively reduce to the case of a closed system, establishing a correspondence between η and r_k . To clearly illustrate this issue, we will first present our constructed wave function as follows:

$$\phi_n = \frac{\operatorname{sech}\eta}{1 + \mu_2 \tanh\eta} |1 - \mu_1^2|^{\frac{n}{2}} \left(\frac{\tanh\eta}{1 + \mu_2 \tanh\eta}\right)^n. \quad (6.13)$$

To perform the Taylor expansion around μ_2 to the first order, we obtain the expression

$$\phi_n \approx |1 - \mu_1^2|^{n/2} \operatorname{sech}(\eta) \tanh^n(\eta) + \mathcal{O}(\mu_2^n).$$

Next, we can neglect the term involving μ_1^2 , which enables us to find that this approximation matches the wave function given in equation (5.2) for $\phi_k = 0$. Additionally, we observe the correspondence $\eta \sim r_k$. In principle, the wave function ϕ_n should incorporate the information of both r_k and ϕ_k to accurately reproduce the wave function represented in (5.2) as the leading order of the open system's method. To achieve this, we will follow the guidelines provided in Appendix D of [10].

For deriving the two-mode squeezed state in open system, we first introduce the concept of orthogonal polynomial sequence (OPS) $\{P_n(x)\}_{n \geq 0}$, it satisfied with the following recurrence relation,

$$P_{n+1}(x) = (x - \tilde{c}_n)P_n(x) - b_n^2 P_{n-1}(x), \quad \text{for } n \geq 1 \quad (6.14)$$

where x represents the Hamiltonian, \tilde{c}_n is associated with the dissipative coefficient, and b_n refers to the Lanczos coefficient. The sequence begins with the initial conditions $P_0(x) = 1$ and $P_1(x) = x - c_0$. For an open system, we have $P_n(x; \alpha, \eta) = \det(x - \mathcal{L}_n)$, where \mathcal{L}_n is the Hamiltonian for the n -th quantum state. This determinant encodes information about b_n as represented by the corresponding matrix. Based on the definition of L , we can express it in terms of x^n or e_n , which will be used to derive the wave function using the open system method.

To obtain the similar recurrence relation as (6.2), we introduce the the natural orthonormal basis $\{e_n\}$, and meanwhile P_n can be represented in terms of e_n

$$P_n(x) = \left(\prod_{k=1}^n b_k \right) e_n, \quad \text{and} \quad x^n = \mathcal{L}^n e_0, \quad (6.15)$$

where x is the parameter of P_n , \mathcal{L} represents our Hamiltonian expressed in terms of creation and annihilation operators, and $|e_n\rangle \equiv |\mathcal{O}_n\rangle = |n_{\vec{k}}; n_{-\vec{k}}\rangle$. By combining Equation (6.14) with Equation (6.15), we can derive the following recurrence relation.

$$b_{n+1}e_{n+1} + b_n e_{n-1} = (x - \tilde{c}_n)e_n. \quad (6.16)$$

Here, x functions as the Hamiltonian. Given the recurrence of P_n , it aligns with the second kind of Meixner polynomials, denoted as $M_n(x; \delta, \eta_1)$. Its generating function is

$$\sum_{n=0}^{\infty} M_n(x; \delta, \eta_1) \frac{t^n}{n!} = ((1 + \delta t^2) + t^2)^{-\eta/2} \exp(x \arctan(\frac{t}{1 + \delta t})) \quad (6.17)$$

The inverse polynomial of $\{M_n(x; \delta, \eta_1)\}_{n \geq 0}$ is $\{Q_n(x; \delta, \eta_1)\}_{n \geq 0}$, which is defined as

$$Q_n(x) = \sum_{k=0}^n \mu_{n,k} x^k, \quad \text{and} \quad x^n = \sum_{k=0}^n \mu_{n,k} P_k(x). \quad (6.18)$$

where $\mu_{n,k}$ refers to a triangular linear transform with matrix elements that relate x to P_n . This formula demonstrates that the polynomials P_n can be expressed in terms of x . All three orthogonal polynomial sequences (OPS) mentioned are examples of Sheffer orthogonal polynomials, which are defined as a set of polynomials $\{P_n(x)\}_{n \geq 0}$ characterized by a generating function,

$$\sum_{n=0}^{\infty} P_n(x) \frac{t^n}{n!} = f(t) \exp(xg(t)). \quad (6.19)$$

And the inverse polynomials are give by

$$\sum_{n=0}^{\infty} Q_n(x) \frac{t^n}{n!} = \frac{1}{f(g^{(-1)}(t))} \exp(xg^{(-1)}(t)), \quad (6.20)$$

where $g^{\langle -1 \rangle}(t)$ stands for the compositional inverse of $g(t)$, which have the following relationship

$$g(g^{\langle -1 \rangle}(t)) = t. \quad (6.21)$$

Back to the Meixner polynomials of the second kind, we find that

$$f(t) = ((1 + \delta t)^2 + t^2)^{-\eta/2}, \quad \text{and} \quad g(t) = \arctan\left(\frac{t}{1 + \delta t}\right). \quad (6.22)$$

Our target function is $Q_n(x)$, and the rationale will be provided in the final derivations. To obtain $Q_n(x)$, we need to know the formula for $g^{\langle -1 \rangle}$. The compositional inverse polynomial of $g(t)$ is

$$t = g(g^{\langle -1 \rangle}(t)) = \arctan\left(\frac{g^{\langle -1 \rangle}(t)}{1 + \delta g^{\langle -1 \rangle}(t)}\right), \quad (6.23)$$

Next,

$$\frac{g^{\langle -1 \rangle}(t)}{1 + \delta g^{\langle -1 \rangle}(t)} = \tan(t) \quad (6.24)$$

And after a few simple calculations,

$$g^{\langle -1 \rangle}(t) = \frac{\tan(t)}{1 - \delta \tan(t)}, \quad (6.25)$$

where δ is a parameter determined by various models. Combine Eqs. (6.25) and (6.20), we obtain the inverse polynomials of $\{M_n(x; \delta, \eta_1)\}_{n \geq 0}$ as following,

$$\sum_{n=0}^{\infty} Q_n(x) \frac{t^n}{n!} = \frac{\sec(t)^{\eta_1}}{(1 - \delta \tan(t))^{\eta_1}} \exp\left(x \frac{\tan(t)}{1 - \delta \tan(t)}\right). \quad (6.26)$$

After the changing the variable as $t = i\eta$ and $\delta = i\mu_2$, where η (conformal time) and μ_2 (dissipation coefficient) are our defined parameters. Making use of $\tan i\eta = i \tanh \eta$ and $\cos i\eta = \cosh \eta$, the generating function of the inverse polynomials become

$$\sum_{n=0}^{\infty} Q_n(x) \frac{(i\eta)^n}{n!} = \frac{\operatorname{sech}(\eta)^{\eta_1}}{(1 + \mu_2 \tanh(\eta))^{\eta_1}} \exp\left(x \frac{i \tanh(\eta)}{1 + \mu_2 \tanh(\eta)}\right). \quad (6.27)$$

Based on Eqs. (6.15) and (6.18), we could obtain

$$(e_d | \mathcal{L}^n | e_0) = \mu_{n,d} \prod_{k=1}^n b_k. \quad (6.28)$$

Furthermore, we could have

$$(e_d | e^{i\mathcal{L}\eta} | e_0) = \prod_{k=1}^d b_k \sum_{n=0}^{\infty} \frac{(i\eta)^n}{n!} \mu_{n,d}. \quad (6.29)$$

In light of (6.18), we could obtain

$$\sum_{n=0}^{\infty} \frac{(i\eta)^n}{n!} \mu_{n,d} = \frac{\operatorname{sech} \eta}{1 + \mu_2 \tanh \eta} \frac{1}{d!} \frac{(i \tanh \eta)^d}{(1 + \mu_2 \tanh \eta)^d}, \quad (6.30)$$

Then we utilize $b_n = \alpha n = \sqrt{|1 - \mu_1^2|}n$ in our case, we naturally get the following formula,

$$(e_n | e^{i\mathcal{L}\eta} | e_0) = \frac{\text{sech}\eta}{1 + \mu_2 \tanh \eta} |1 - \mu_1^2|^{\frac{n}{2}} \frac{(i \tanh \eta)^n}{(1 + \mu_2 \tanh \eta)^n} \quad (6.31)$$

thus, we obtain the wave function

$$|\mathcal{O}(t)\rangle = e^{i\mathcal{L}\eta} |e_0\rangle = \frac{\text{sech}\eta}{1 + \mu_2 \tanh \eta} \sum_{n=0}^{\infty} |1 - \mu_1^2|^{\frac{n}{2}} \frac{(-1 \exp(2i\phi_k(\eta)) \tanh \eta)^n}{(1 + \mu_2 \tanh \eta)^n} |e_n\rangle$$

where

$$|\mathcal{O}_n\rangle = |e_n\rangle$$

In our calculations, we multiply a phase factor $ie^{2i\phi_k(\eta)}$ which does not alter the wave function. Finally, we can set $r_k = \eta$, allowing us to denote the two-mode squeezed state within the open system as,

$$\phi_n(\eta) = (-1)^n e^{2in\phi_k} \frac{\text{sech}r_k}{1 + \mu_2 \tanh r_k} |1 - \mu_1^2|^{\frac{n}{2}} \frac{(\tanh r_k)^n}{(1 + \mu_2 \tanh r_k)^n}. \quad (6.32)$$

This wave function is our central result in this paper whose leading order of ϕ_n in terms of μ_2 is consistent with the wave function described in (5.2). The idea of changing the variable is borrowed from the construction of coherent states, where a key component is the generation of the displacement operator, defined as $D(\eta) = e^{iHt}$, with H being the corresponding Hamiltonian, where one can change t in terms of r_k and ϕ_k . In Ref. [12], it is stated that the generalized coherent state is derived by constructing a generalized displacement operator according to their group representation theory.

6.4 The power of wave function (6.32)

We discuss the two-mode squeezed state in an open system, as described in equation (6.32). Unlike the two-mode squeezed state derived from closed system methods, our wave function (6.32) is more realistic, as it considers a vast open environment. Additionally, although our derivation pertains to the early universe, this wave function can also be applied to fields such as quantum optics, quantum information, and condensed matter physics, where information is encoded in the parameters μ_1 and μ_2 determined by the specific Hamiltonian. Finally, we observe that our calculations hold true by requiring that the recurrence relation (6.14) which is equivalent to the Lanczos algorithm. This connection highlights the power of the Lanczos algorithm, which provides a natural method for constructing the wave function according to their Hamiltonian, even for open systems.

6.5 The evolution of $r_k(\eta)$ and $\phi_k(\eta)$ in open system's method

According to the standard procedure, we need to derive the evolution equations for r_k and ϕ_k in relation to conformal time η . The detailed calculations for this derivation can be

found in Appendix A. The evolution can be summarized as follows:

$$\begin{aligned}
r'_k &= \frac{|1 - \mu_1^2|^{\frac{1}{2}} \sinh 2r_k \left(\frac{a^2 V_{,\phi\phi}}{2k} \sin 2\phi_k - \frac{a'}{a} \cos 2\phi_k \right) - \sinh 2r_k \mu'_2}{(\sinh 2r_k + 2\mu_2 \cosh^2 r_k)} \\
\phi'_k &= - \left(k + \frac{a^2 V_{,\phi\phi}}{2k} \right) + \frac{1}{2} \left(\frac{a^2 V_{,\phi\phi}}{2k} \cos 2\phi_k + \frac{a'}{a} \sin 2\phi_k \right) \\
&\quad \left[|1 - \mu_1^2|^{\frac{1}{2}} \frac{\tanh r_k}{1 + \mu_2 \tanh r_k} + |1 - \mu_1^2|^{-\frac{1}{2}} (\tanh^{-1} r_k + \mu_2) \right],
\end{aligned} \tag{6.33}$$

where prime denotes the varying with respect to the conformal time η . The same as the closed system, we change variable as $y = \log_{10} a$, the evolution equation of r_k and ϕ_k will become as,

$$\begin{aligned}
\frac{H_0}{\ln 10} 10^{-\frac{y}{2}(1+3\omega)} \frac{dr_k}{dy} &= \frac{|1 - \mu_1^2|^{\frac{1}{2}} \sinh 2r_k \left(\frac{10^{2y} V_{,\phi\phi}}{2k} \sin 2\phi_k - H_0 10^{-\frac{y}{2}(1+3\omega)} \cos 2\phi_k \right) - \sinh 2r_k \mu'_2}{(\sinh 2r_k + 2\mu_2 \cosh^2 r_k)} \\
\frac{H_0}{\ln 10} 10^{-\frac{y}{2}(1+3\omega)} \frac{d\phi_k}{dy} &= - \left(k + \frac{10^{2y} V_{,\phi\phi}}{2k} \right) + \frac{1}{2} \left(\frac{10^{2y} V_{,\phi\phi}}{2k} \cos 2\phi_k + H_0 10^{-\frac{y}{2}(1+3\omega)} \sin 2\phi_k \right) \\
&\quad \left[|1 - \mu_1^2|^{\frac{1}{2}} \frac{\tanh r_k}{1 + \mu_2 \tanh r_k} + |1 - \mu_1^2|^{-\frac{1}{2}} (\tanh^{-1} r_k + \mu_2) \right]
\end{aligned} \tag{6.34}$$

where

$$\begin{aligned}
\mu_2 &= k + \frac{10^{2y} V_{,\phi\phi}}{2k}, \quad \mu'_2 = H_0 10^{-\frac{y}{2}(1+3\omega)} \frac{10^{2y} V_{,\phi\phi}}{k} + \frac{10^{2y} V'_{,\phi\phi}}{2k} \\
|1 - \mu_1^2| &= \left(\frac{10^{2y} V_{,\phi\phi}}{2k} \right)^2 + \left(H_0 10^{-\frac{y}{2}(1+3\omega)} \right)^2.
\end{aligned}$$

During the calculations, we accounted for the background of ϕ using conformal time η , as demonstrated by the various potentials in Eq. (3.11). Consequently, μ_2 and μ_1 also vary with respect to conformal time, since they include contributions from the potential and the scale factor a .

Fig. 8 clearly illustrates the evolution of r_k across various epochs, including inflation, radiation domination (RD), and matter domination (MD). It is evident that the different potentials produce similar trends for r_k . Unlike in Fig. 3, there is no oscillation of r_k once dissipation effects are considered. Additionally, the trend of r_k varies, particularly during the MD phase, where the evolution consistently shows an increase. These differences will result in distinctive evolutions of Krylov complexity and Krylov entropy.

6.6 Krylov complexity and Krylov entropy with the approach of open system

In this section, we will continue use the wave function (6.32) to explore the Krylov complexity and Krylov entropy. All of these calculation are exactly the same with our previous study [57], the only differences is that we need to use r_k to take place of η in the formulas for Krylov complexity and Krylov entropy whose formulas can be expressed as following:

$$K = \frac{\text{sech}^2 r_k |1 - \mu_1^2| \tanh^2 r_k}{[1 + 2\mu_2 \tanh r_k + (\mu_2^2 - |1 - \mu_1^2|) \tanh^2 r_k]^2} \tag{6.35}$$

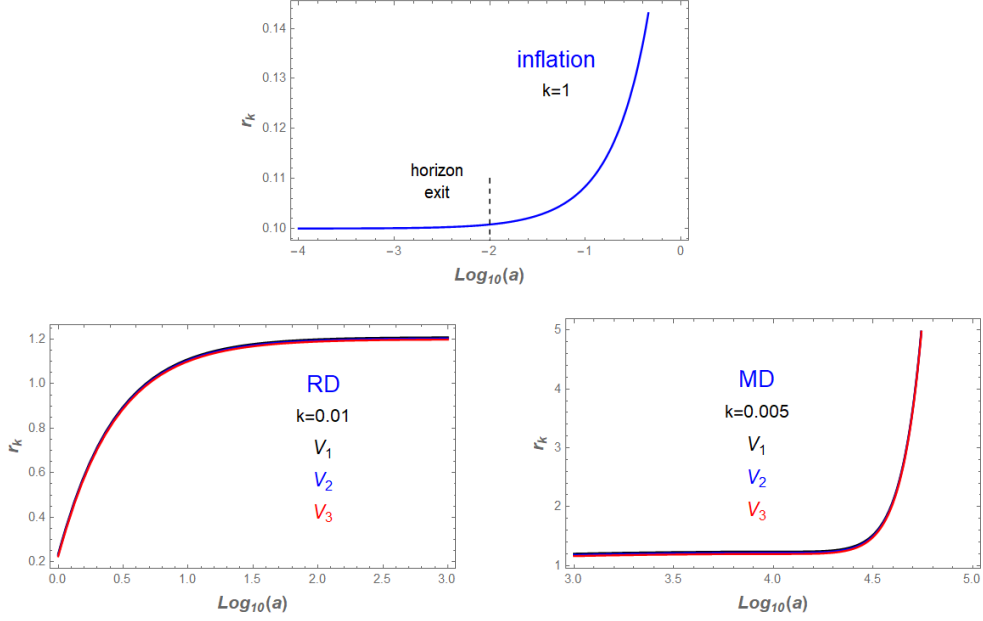


Figure 8. The numerical of r_k in terms of $\log_{10} a$ for three different periods (inflation, RD, and MD), where we set $H_0 = 1$. $k = 1$ at period inflation, $k = 0.01$ at period RD, $k = 0.005$ at period MD for simplicity.

and

$$\begin{aligned}
S_k = \frac{\text{sech}^2 r_k}{A^2} & \left[(1 + \mu_2 \tanh r_k)^2 \ln(1 + \mu_2 \tanh r_k)^2 - \tanh^2 r_k |1 - \mu_1^2| \ln \tanh^2 r_k \right. \\
& \left. - [(1 + \mu_2 \tanh r_k)^2 - |1 - \mu_1^2| \tanh^2 r_k] \ln \text{sech}^2 r_k - \tanh^2 r_k |1 - \mu_1^2| \ln |1 - \mu_1^2| \right]
\end{aligned} \tag{6.36}$$

where we have defined $A = 1 + 2\mu_2 \tanh r_k + (\mu_2^2 - |1 - \mu_1^2|) \tanh^2 r_k$ for simplicity. It straightforwardly demonstrates the leading order of Krylov complexity (6.35) and Krylov entropy (6.36) will nicely recover into the case of Eq. (5.3) and Eq. (5.4) under the weak dissipative approximation, namely, $\mu_2 \ll 1$.

Fig. 9 illustrates the evolution of Krylov complexity during inflation, radiation domination (RD), and matter domination (MD). During inflation, we observe that Krylov complexity increases exponentially, which is consistent with the closed system's method. However, the trends in RD and MD differ from those shown in Fig. 4, where the complexity tends to stabilize around certain constant values, oscillating around these values in both RD and MD. In the case of an open system, it is evident that Krylov complexity decreases during RD. For MD, Krylov complexity initially peaks as the scale factor a increases and then declines to stabilize at constant values. Additionally, it is noteworthy that the order of Krylov complexity in an open system is significantly lower than in a closed system, even in RD and MD. Our numerical analysis shows that the term $\text{sech}(r_k)$ in Eq. (6.35) leads to this outcome, regardless of whether the system is weakly dissipative or not. We have demonstrated that both RD and MD can be approximated as weakly dissipative systems

under the condition $\mu < 1$. Recalling the meaning of Krylov complexity, it describes the operator growth in a many-body system and our early universe is a perfect chaotic system due to $b_n = \alpha n$. Our numeric reveals that the operator growth is much smaller compared with the case of a closed system, which is consistent with reality since the dissipation will lead to faster decreasing of operator growth compared with that without the dissipation effects.

Once one understands the role of dissipation effects, it becomes evident that the order of Krylov entropy in an open system is lower compared to that in a closed system, as illustrated in Figs 10 and 5. The evolution trend is particularly distinctive for RD and MD, as shown in Figure 10, where the Krylov entropy initially peaks before stabilizing at constant values. In the case of MD, the Krylov entropy initially holds steady at certain values before decreasing to some constant level. Overall, the background conditions and dissipative effects have a significant impact on both Krylov complexity and Krylov entropy.

In this section, we utilized the wave function presented in Eq. (6.32) to investigate Krylov complexity and Krylov entropy. By comparing our findings to those from a closed system, we observed that the dissipative effects not only influence the overall evolution of the system but also reduce the order of Krylov complexity and Krylov entropy. Since Krylov complexity reflects the growth of operators—a fundamental quantum property of a dynamical system—we can conclude that, when the growth of the operator is diminished in the open system compared to the closed system, the dissipative effects lead to a more rapid decoherence-like behavior. Meanwhile, we also could see that the various potentials will almost produce the same trend of Krylov complexity and Krylov entropy in different epochs.

7 Summary and outlook

The definition of Krylov complexity is clear and unambiguous, especially when compared to circuit complexity. Its uniqueness eliminates the need for introducing a parametric manifold to illustrate the concept of complexity. Additionally, Krylov complexity characterizes the growth of operations within a dynamical system, and the order of Krylov complexity can indicate the quantum level of that system. Krylov complexity is rooted in the Lanczos algorithm, a powerful method for assessing the nature of dynamical systems, which can be chaotic, integrable, or free. The key criteria for this assessment is the Lanczos coefficient, whose formula indicates the characteristics of a given dynamical system. For example, the relation $b = \alpha n$ suggests that the system is chaotic. In our paper, we highlight that the Lanczos coefficient effectively reveals that our early universe was a many-body, infinite, and chaotic system. From a cosmological perspective, the universe is considered an entirely open system. Notably, the Lanczos algorithm offers a natural way to construct the wave function of an open system using the second kind of Meixner polynomials. Given these insights, it is particularly important to explore Krylov complexity throughout the early universe, including inflation, RD and MD.

In this paper, we thoroughly examine Krylov complexity in both open and closed system methods. Our primary result is the derivation of the two-mode squeezed state

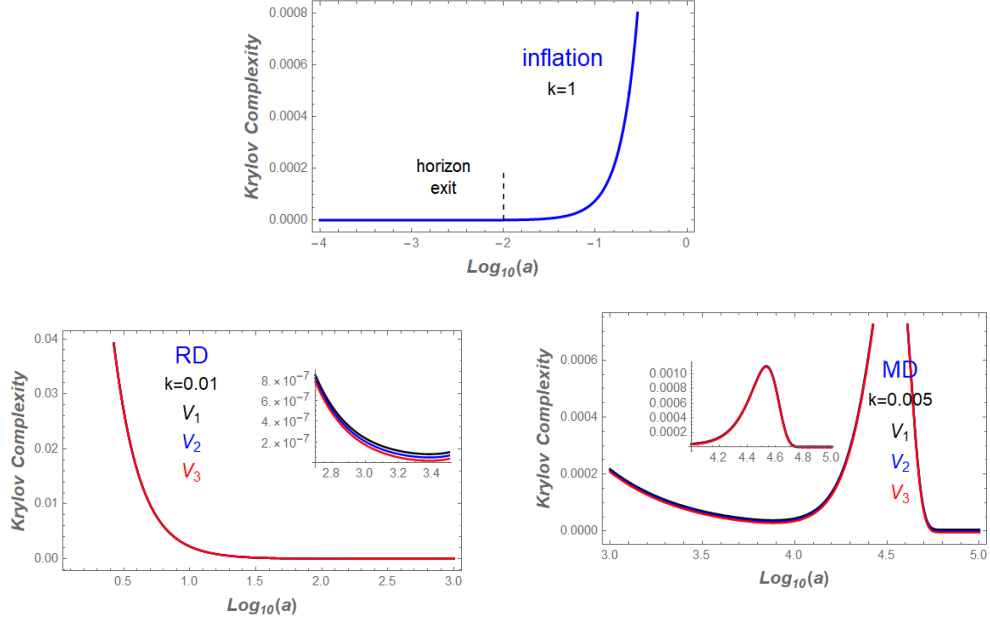


Figure 9. The numerical of Krylov complexity in terms of $\log_{10} a$ for three different periods (inflation, RD, and MD), where we set $H_0 = 1$, $k = 0.01$ at period inflation and RD, $k = 0.005$ at period MD for simplicity.

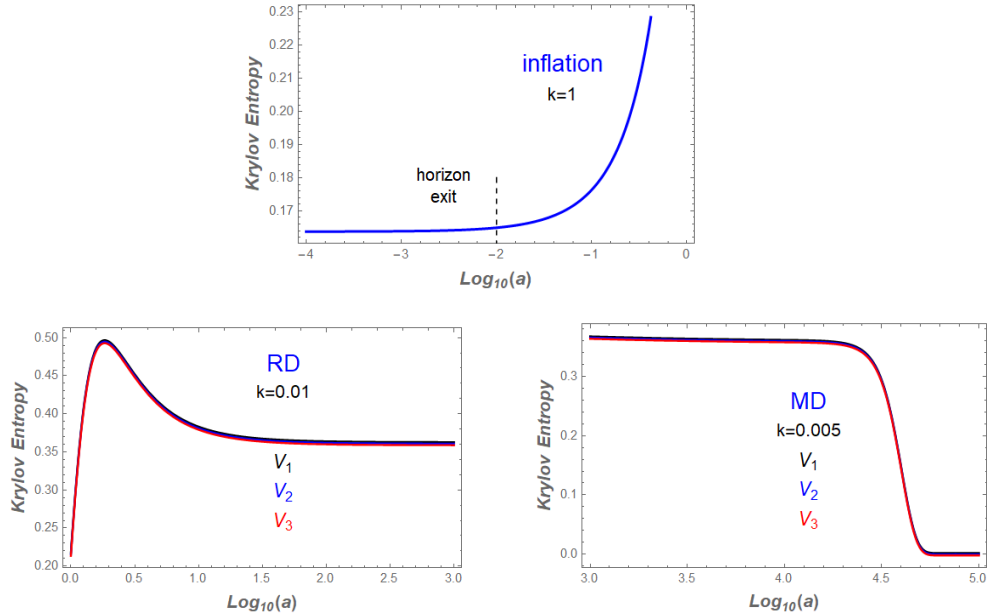


Figure 10. The numerical of Krylov entropy in terms of $\log_{10} a$ for three different periods (inflation, RD, and MD), where we set $H_0 = 1$, $k = 0.01$ at period inflation and RD, $k = 0.005$ at period MD for simplicity.

using the open system approach, along with the calculation of its evolution equations for $\phi_k(\eta)$ and $r_k(\eta)$. Below, we present our key findings.

(a). In Sec. 2, we introduce the Lanczos algorithm and the associated Lanczos coefficients, which apply equally to both open and closed systems. As noted by [10], the Liouvillian superoperator acts as the Hamiltonian when it can be expressed in terms of creation and annihilation operators. Our exploration of Krylov complexity encompasses the entire universe, including inflation, RD, MD, and the violations of slow-roll conditions, which necessitates considering contributions from potential energy. Sec. 3 discusses the most common potentials, such as the Higgs potential, Starobinsky’s inflationary potential, and chaotic inflationary potential. These models encompass a wide range of inflationary scenarios due to the unifying characteristics of α attractors. To accurately capture the information pertaining to these potentials, we examine the dynamics of the field ϕ in relation to the scale factor during the preheating process, as represented in Eq. (3.9). From these calculations, we determine the effective mass for various inflationary potentials, as illustrated in Fig. 2. Our findings indicate that the potential approaches certain constant values during RD and MD.

(b). In light of the scale factor and various potentials, we examine Krylov complexity using the closed system method. First, we numerically simulate the r_k of the two-mode squeezed state, as depicted in Fig. 3. The simulation shows oscillations during inflation, which are enhanced in RD and MD, maintaining some constant values. Notably, the different potentials produce almost identical trends for r_k . Based on the numerical results for r_k , we also simulate the corresponding Krylov complexity and Krylov entropy, as illustrated in Figs. 4 and 5. The trends of both Krylov complexity and Krylov entropy are similar across the corresponding epochs. During inflation, we observe exponential growth, consistent with our previous study [57]. In the RD and MD phases, the trends show initial enhancement before saturating to constant values. Additionally, various inflationary models exhibit nearly the same trends for Krylov complexity and Krylov entropy, confirming the approximation that the effective mass of the inflaton is approximately constant, as indicated in [59].

(c). Within the method of an open system, we rigorously derive the wave function of an open system using the second kind of Meixner polynomials, which we name it as the open two-mode squeezed state. This derivation is represented in Eq. (6.32). Throughout this process, we discover that the Lanczos coefficient b_n and the dissipative coefficient are precisely determined by the specific Hamiltonian, leading to the conclusion that b_n is identical across both methods. Our findings indicate that $b_n = \alpha n$, suggesting that our universe behaves as an entirely chaotic system. Consequently, the Lyapunov index is equivalent to b_n when $n = 2$. Figure 6 illustrates the chaos present across various epochs. During the inflationary period, chaos increases exponentially before diminishing to a certain level, only to rise again due to the preheating process. Additionally, we examine the evolution of the dissipative coefficient in RD and MD. This analysis builds on previous work in Ref. [57], which discusses the strong dissipative nature of the system during inflation. From Fig. 7, we can confirm that the RD and MD systems are weakly dissipative, characterized by $\mu_2 \ll 1$.

Additionally, we derive the evolution of r_k and ϕ_k , noting that the solution for r_k is dependent on the solution for ϕ_k due to their coupling, as described by Eq. (6.33). Using the wave function in Eq. (6.32), we calculate the Krylov complexity and Krylov entropy, which are represented in Eqs. (6.35) and (6.36). The leading order of these quantities aligns well with the formulas derived from the closed system method. In accordance with standard procedures, we need the numerical values of r_k within the open system framework, as illustrated in Fig. 8. Unlike the closed system, there is no oscillation observed for r_k during inflation, and the trends of Krylov complexity and Krylov entropy are depicted in Figs. 9 and 10. Compared to the closed system method, we observe that the values of Krylov complexity and Krylov entropy are significantly smaller. Recalling the definition of Krylov complexity, which pertains to the operator growth in a dynamical system, we find that a smaller operator growth suggests a decoherence-like behavior within the Krylov complexity. When dissipative effects are considered, we observe decoherence-like behavior, whether the system is weakly dissipative or not.

While we have achieved a comprehensive understanding of Krylov complexity in the early universe, many ideas still remain to be explored. Here, we outline several future directions.

Firstly, we investigate the Krylov complexity in the context of single-field inflation, and it is quite natural to extend our work into the multi-field framework [76–79] as well as $f(R)$ gravity [80–82]. This extension allows us to explore the geometrical effects of fields and higher orders of Ricci curvature on Krylov complexity. Our Hamiltonian, given by (4.10), is Hermitian and includes the component of an open system. The traditional approach to handling open systems in quantum mechanics involves constructing what is known as a Lindbladian [83, 84], where the corresponding Hamiltonian is non-Hermitian. In our case, a natural method is to expand the action to higher orders with respect to the Mukhanov-Sasaki variable.

Secondly, our results indicate that the Krylov complexity in a weak dissipative system (RD or MD) will not follow the general discussions mentioned in Sec. 6.2. One possible explanation for this discrepancy is the neglect of decoherence in curvature perturbation during horizon exits. Ref. [75] suggests that decoherence in circuit complexity may lead to this phenomenon of saturation. A similar concept might apply to Krylov complexity, particularly concerning the role of decoherence in the construction of the wave function.

Thirdly, we have already obtained the open two-mode squeezed state as described in (6.32). In light of this wave function, we can explore several additional avenues. For instance, we can calculate the two-point correlation functions to derive the power spectrum. Since the derivation of this wave function is model-independent, we have the flexibility to utilize different models of this wave function to test its validity. Conversely, we can also constrain the parameters μ_1 and μ_2 based on data from the Cosmic Microwave Background (CMB). Furthermore, it is important to highlight that Ref. [56] indicates the potential application of the CV conjecture to Krylov complexity during inflation; however, their approach is tailored for a closed system. In contrast, our universe is fundamentally an open system, which provides us with the opportunity to further investigate the validity of the CV conjecture for Krylov complexity within the context of open systems.

Acknowledgments

LH and KH are funded by NSFC grant NO. 12165009, Hunan Natural Science Foundation NO. 2023JJ30487 and NO. 2022JJ40340.

A The calculation of r_k and ϕ_k within the method of open system

In this appendix, we will give the detailed calculations for r_k and ϕ_k based on the open two-mode squeezed state,

$$|\psi\rangle = \frac{\text{sech } r_k}{1 + \mu_2 \tanh r_k} \sum_{n=0}^{\infty} (-1)^n |1 - \mu_1^2|^{\frac{n}{2}} e^{2in\phi_k} \left(\frac{\tanh r_k}{1 + \mu_2 \tanh r_k} \right)^n |n, n\rangle_{\vec{k}, -\vec{k}} \quad (\text{A.1})$$

We will write down our Hamiltonian (4.10) as follows,

$$\hat{H} = \left(k + \frac{a^2 V_{,\phi\phi}}{2k} \right) (\hat{c}_{\vec{k}} \hat{c}_{\vec{k}}^\dagger + \hat{c}_{-\vec{k}}^\dagger \hat{c}_{-\vec{k}}) + \left(\frac{a^2 V_{,\phi\phi}}{2k} + i \frac{a'}{a} \right) \hat{c}_{-\vec{k}}^\dagger \hat{c}_{\vec{k}}^\dagger + \left(\frac{a^2 V_{,\phi\phi}}{2k} - i \frac{a'}{a} \right) \hat{c}_{-\vec{k}} \hat{c}_{\vec{k}} \quad (\text{A.2})$$

According to the Schrödinger equation $\hat{H}\psi = i\partial_\eta\psi$ ($\hbar = 1$), we first calculate the left hand side of Schrödinger equation as follows,

$$\begin{aligned} \hat{H}|\psi\rangle &= \frac{\text{sech } r_k}{1 + \mu_2 \tanh r_k} \sum_{n=0}^{\infty} (-1)^n |1 - \mu_1^2|^{\frac{n}{2}} e^{2in\phi_k} \left(\frac{\tanh r_k}{1 + \mu_2 \tanh r_k} \right)^n \left[\left(k + \frac{a^2 V_{,\phi\phi}}{2k} \right) (\hat{c}_{\vec{k}} \hat{c}_{\vec{k}}^\dagger \right. \\ &\quad \left. + \hat{c}_{-\vec{k}}^\dagger \hat{c}_{-\vec{k}}) |n, n\rangle_{\vec{k}, -\vec{k}} + \left(\frac{a^2 V_{,\phi\phi}}{2k} + i \frac{a'}{a} \right) \hat{c}_{-\vec{k}}^\dagger \hat{c}_{\vec{k}}^\dagger |n, n\rangle_{\vec{k}, -\vec{k}} + \left(\frac{a^2 V_{,\phi\phi}}{2k} - i \frac{a'}{a} \right) \hat{c}_{-\vec{k}} \hat{c}_{\vec{k}} |n, n\rangle_{\vec{k}, -\vec{k}} \right] \\ &= \frac{\text{sech } r_k}{1 + \mu_2 \tanh r_k} \sum_{n=0}^{\infty} (-1)^n |1 - \mu_1^2|^{\frac{n}{2}} e^{2in\phi_k} \left(\frac{\tanh r_k}{1 + \mu_2 \tanh r_k} \right)^n \left[\left(k + \frac{a^2 V_{,\phi\phi}}{2k} \right) (2n + 1) \right. \\ &\quad \left. |n, n\rangle_{\vec{k}, -\vec{k}} + \left(\frac{a^2 V_{,\phi\phi}}{2k} + i \frac{a'}{a} \right) (n + 1) |n + 1, n + 1\rangle_{\vec{k}, -\vec{k}} + \left(\frac{a^2 V_{,\phi\phi}}{2k} - i \frac{a'}{a} \right) n |n - 1, n - 1\rangle_{\vec{k}, -\vec{k}} \right] \\ &= \frac{\text{sech } r_k}{1 + \mu_2 \tanh r_k} \left[\left(k + \frac{a^2 V_{,\phi\phi}}{2k} \right) - |1 - \mu_1^2|^{\frac{1}{2}} e^{2i\phi_k} \frac{\tanh r_k}{1 + \mu_2 \tanh r_k} \left(\frac{a^2 V_{,\phi\phi}}{2k} - i \frac{a'}{a} \right) \right] |0, 0\rangle_{\vec{k}, -\vec{k}} \\ &\quad + \frac{\text{sech } r_k}{1 + \mu_2 \tanh r_k} \left[\left(k + \frac{a^2 V_{,\phi\phi}}{2k} \right) - |1 - \mu_1^2|^{\frac{1}{2}} e^{2i\phi_k} \frac{\tanh r_k}{1 + \mu_2 \tanh r_k} \left(\frac{a^2 V_{,\phi\phi}}{2k} - i \frac{a'}{a} \right) \right] \\ &\quad \sum_{n=1}^{\infty} (-1)^n |1 - \mu_1^2|^{\frac{n}{2}} e^{2in\phi_k} \left(\frac{\tanh r_k}{1 + \mu_2 \tanh r_k} \right)^n |n, n\rangle_{\vec{k}, -\vec{k}} + \frac{\text{sech } r_k}{1 + \mu_2 \tanh r_k} \left[\left(2k + \frac{a^2 V_{,\phi\phi}}{k} \right) \right. \\ &\quad \left. - |1 - \mu_1^2|^{\frac{1}{2}} e^{2i\phi_k} \frac{\tanh r_k}{1 + \mu_2 \tanh r_k} \left(\frac{a^2 V_{,\phi\phi}}{2k} - i \frac{a'}{a} \right) - |1 - \mu_1^2|^{-\frac{1}{2}} e^{-2i\phi_k} \left(\frac{\tanh r_k}{1 + \mu_2 \tanh r_k} \right)^{-1} \right. \\ &\quad \left. \left(\frac{a^2 V_{,\phi\phi}}{2k} + i \frac{a'}{a} \right) \right] \sum_{n=1}^{\infty} (-1)^n n |1 - \mu_1^2|^{\frac{n}{2}} e^{2in\phi_k} \left(\frac{\tanh r_k}{1 + \mu_2 \tanh r_k} \right)^n |n, n\rangle_{\vec{k}, -\vec{k}} \end{aligned} \quad (\text{A.3})$$

Then, the right hand side is following as,

$$\begin{aligned}
i \frac{d}{d\eta} |\psi\rangle &= i \frac{d}{d\eta} \left[\frac{\operatorname{sech} r_k}{1 + \mu_2 \tanh r_k} \sum_{n=0}^{\infty} (-1)^n |1 - \mu_1^2|^{\frac{n}{2}} e^{2in\phi_k} \left(\frac{\tanh r_k}{1 + \mu_2 \tanh r_k} \right)^n |n, n\rangle_{\vec{k}, -\vec{k}} \right] \\
&= i \left[- \frac{(\sinh 2r_k + 2\mu_2 \cosh^2 r_k) r'_k + \sinh 2r_k \mu'_2}{2 \cosh^3 r_k (1 + \mu_2 \tanh r_k)^2} \sum_{n=0}^{\infty} (-1)^n |1 - \mu_1^2|^{\frac{n}{2}} e^{2in\phi_k} \left(\frac{\tanh r_k}{1 + \mu_2 \tanh r_k} \right)^n \right. \\
&\quad \left. |n, n\rangle_{\vec{k}, -\vec{k}} \right] + i \left[\frac{\operatorname{sech} r_k}{1 + \mu_2 \tanh r_k} \sum_{n=0}^{\infty} (-1)^n |1 - \mu_1^2|^{\frac{n}{2}} e^{2in\phi_k} \left(\frac{\tanh r_k}{1 + \mu_2 \tanh r_k} \right)^n \right. \\
&\quad \left. \left[2i\phi'_k + \frac{2r'_k}{\sin 2r_k (1 + \mu_2 \tanh r_k)} + \frac{|1 - \mu_1^2|'}{2|1 - \mu_1^2|} - \frac{\tanh r_k \mu'_2}{1 - \mu_2 \tanh r_k} \right] |n, n\rangle_{\vec{k}, -\vec{k}} \right] \\
&= -i \frac{(\sinh 2r_k + 2\mu_2 \cosh^2 r_k) r'_k + \sinh 2r_k \mu'_2}{2 \cosh^3 r_k (1 + \mu_2 \tanh r_k)^2} |0, 0\rangle_{\vec{k}, -\vec{k}} \\
&\quad - i \frac{(\sinh 2r_k + 2\mu_2 \cosh^2 r_k) r'_k + \sinh 2r_k \mu'_2}{2 \cosh^3 r_k (1 + \mu_2 \tanh r_k)^2} \sum_{n=1}^{\infty} (-1)^n |1 - \mu_1^2|^{\frac{n}{2}} e^{2in\phi_k} \left(\frac{\tanh r_k}{1 + \mu_2 \tanh r_k} \right)^n \\
&\quad |n, n\rangle_{\vec{k}, -\vec{k}} + \frac{\operatorname{sech} r_k}{1 + \mu_2 \tanh r_k} \left(-2\phi'_k + i \frac{2r'_k}{\sin 2r_k (1 + \mu_2 \tanh r_k)} + i \frac{|1 - \mu_1^2|'}{2|1 - \mu_1^2|} \right. \\
&\quad \left. - i \frac{\tanh r_k \mu'_2}{1 - \mu_2 \tanh r_k} \right) \sum_{n=1}^{\infty} (-1)^n n |1 - \mu_1^2|^{\frac{n}{2}} e^{2in\phi_k} \left(\frac{\tanh r_k}{1 + \mu_2 \tanh r_k} \right)^n |n, n\rangle_{\vec{k}, -\vec{k}}
\end{aligned} \tag{A.4}$$

In combination with Eq. (A.3) and Eq. (A.4), the Schrödinger equation for the squeezed state of the open system is simplified as follows,

$$\begin{aligned}
&A_1 |0, 0\rangle_{\vec{k}, -\vec{k}} + A_1 \sum_{n=1}^{\infty} (-1)^n |1 - \mu_1^2|^{\frac{n}{2}} e^{2in\phi_k} \left(\frac{\tanh r_k}{1 + \mu_2 \tanh r_k} \right)^n |n, n\rangle_{\vec{k}, -\vec{k}} \\
&\quad + A_2 \sum_{n=1}^{\infty} (-1)^n n |1 - \mu_1^2|^{\frac{n}{2}} e^{2in\phi_k} \left(\frac{\tanh r_k}{1 + \mu_2 \tanh r_k} \right)^n |n, n\rangle_{\vec{k}, -\vec{k}} \\
&= B_1 |0, 0\rangle_{\vec{k}, -\vec{k}} + B_1 \sum_{n=1}^{\infty} (-1)^n |1 - \mu_1^2|^{\frac{n}{2}} e^{2in\phi_k} \left(\frac{\tanh r_k}{1 + \mu_2 \tanh r_k} \right)^n |n, n\rangle_{\vec{k}, -\vec{k}} \\
&\quad + B_2 \sum_{n=1}^{\infty} (-1)^n n |1 - \mu_1^2|^{\frac{n}{2}} e^{2in\phi_k} \left(\frac{\tanh r_k}{1 + \mu_2 \tanh r_k} \right)^n |n, n\rangle_{\vec{k}, -\vec{k}}.
\end{aligned} \tag{A.5}$$

Thus, we obtain $A_1 = B_1$ as

$$\begin{aligned}
&-i \frac{(\sinh 2r_k + 2\mu_2 \cosh^2 r_k) r'_k + \sinh 2r_k \mu'_2}{2 \cosh^3 r_k (1 + \mu_2 \tanh r_k)^2} \\
&= \frac{\operatorname{sech} r_k}{1 + \mu_2 \tanh r_k} \left[\left(k + \frac{a^2 V_{,\phi\phi}}{2k} \right) - |1 - \mu_1^2|^{\frac{1}{2}} e^{2i\phi_k} \frac{\tanh r_k}{1 + \mu_2 \tanh r_k} \left(\frac{a^2 V_{,\phi\phi}}{2k} - i \frac{a'}{a} \right) \right],
\end{aligned} \tag{A.6}$$

and we're concerned about the imaginary component,

$$\begin{aligned}
& -i \frac{(\sinh 2r_k + 2\mu_2 \cosh^2 r_k)r'_k + \sinh 2r_k \mu'_2}{2 \cosh^3 r_k (1 + \mu_2 \tanh r_k)^2} \\
& = -\frac{\operatorname{sech} r_k}{1 + \mu_2 \tanh r_k} \left[|1 - \mu_1^2|^{\frac{1}{2}} \frac{\tanh r_k}{1 + \mu_2 \tanh r_k} \left(\frac{a^2 V_{,\phi\phi}}{2k} \sin 2\phi_k - \frac{a'}{a} \cos 2\phi_k \right) \right].
\end{aligned} \tag{A.7}$$

and therefore, we could obtain the evolution of r_k as,

$$r'_k = \frac{|1 - \mu_1^2|^{\frac{1}{2}} \sinh 2r_k \left(\frac{a^2 V_{,\phi\phi}}{2k} \sin 2\phi_k - \frac{a'}{a} \cos 2\phi_k \right) - \sinh 2r_k \mu'_2}{(\sinh 2r_k + 2\mu_2 \cosh^2 r_k)}. \tag{A.8}$$

The other side, we have $A_2 = B_2$ showing as

$$\begin{aligned}
& \frac{\operatorname{sech} r_k}{1 + \mu_2 \tanh r_k} \left[-2\phi'_k + i \frac{2r'_k}{\sin 2r_k (1 + \mu_2 \tanh r_k)} + i \frac{|1 - \mu_1^2|'}{2|1 - \mu_1^2|} - i \frac{\tanh r_k \mu'_2}{1 - \mu_2 \tanh r_k} \right] \\
& = \frac{\operatorname{sech} r_k}{1 + \mu_2 \tanh r_k} \left[\left(2k + \frac{a^2 V_{,\phi\phi}}{k} \right) - |1 - \mu_1^2|^{\frac{1}{2}} e^{2i\phi_k} \frac{\tanh r_k}{1 + \mu_2 \tanh r_k} \left(\frac{a^2 V_{,\phi\phi}}{2k} - i \frac{a'}{a} \right) \right. \\
& \quad \left. - |1 - \mu_1^2|^{-\frac{1}{2}} e^{-2i\phi_k} \left(\frac{\tanh r_k}{1 + \mu_2 \tanh r_k} \right)^{-1} \left(\frac{a^2 V_{,\phi\phi}}{2k} + i \frac{a'}{a} \right) \right],
\end{aligned} \tag{A.9}$$

the real component can read as,

$$\begin{aligned}
& -\frac{2\phi'_k \operatorname{sech} r_k}{1 + \mu_2 \tanh r_k} = \frac{\operatorname{sech} r_k}{1 + \mu_2 \tanh r_k} \left[\left(2k + \frac{a^2 V_{,\phi\phi}}{k} \right) \right. \\
& \quad \left. - \left(\frac{a^2 V_{,\phi\phi}}{2k} \cos 2\phi_k + \frac{a'}{a} \sin 2\phi_k \right) \left(|1 - \mu_1^2|^{\frac{1}{2}} \frac{\tanh r_k}{1 + \mu_2 \tanh r_k} + |1 - \mu_1^2|^{-\frac{1}{2}} (\tanh^{-1} r_k + \mu_2) \right) \right].
\end{aligned} \tag{A.10}$$

Finally, we could obtain the evolution equation of ϕ_k as follows,

$$\begin{aligned}
\phi'_k = & -\left(k + \frac{a^2 V_{,\phi\phi}}{2k} \right) + \frac{1}{2} \left(\frac{a^2 V_{,\phi\phi}}{2k} \cos 2\phi_k + \frac{a'}{a} \sin 2\phi_k \right) \\
& \left[|1 - \mu_1^2|^{\frac{1}{2}} \frac{\tanh r_k}{1 + \mu_2 \tanh r_k} + |1 - \mu_1^2|^{-\frac{1}{2}} (\tanh^{-1} r_k + \mu_2) \right].
\end{aligned} \tag{A.11}$$

One can easily check that Eqs. (A.8) and (A.11) could nicely recover into Eq. (4.12) as $\mu_1 = \mu_2 = 0$.

References

- [1] D. Stanford and L. Susskind, Phys. Rev. D **90** (2014) no.12, 126007 doi:10.1103/PhysRevD.90.126007 [arXiv:1406.2678 [hep-th]].
- [2] T. Hartman and J. Maldacena, JHEP **05** (2013), 014 doi:10.1007/JHEP05(2013)014 [arXiv:1303.1080 [hep-th]].
- [3] H. Liu and S. J. Suh, Phys. Rev. Lett. **112** (2014), 011601 doi:10.1103/PhysRevLett.112.011601 [arXiv:1305.7244 [hep-th]].
- [4] S. Aaronson, [arXiv:1607.05256 [quant-ph]].

- [5] M. A. Nielsen, *Quant. Inf. Comput.* **6** (2006) no.3, 213-262 doi:10.26421/QIC6.3-2 [arXiv:quant-ph/0502070 [quant-ph]].
- [6] M. R. Dowling and M. A. Nielsen, *Quant. Inf. Comput.* **8** (2008) no.10, 0861-0899 doi:10.26421/QIC8.10-1 [arXiv:quant-ph/0701004 [quant-ph]].
- [7] M. A. Nielsen, M. R. Dowling, M. Gu and A. C. Doherty, *Science* **311** (2006) no.5764, 1133-1135 doi:10.1126/science.1121541 [arXiv:quant-ph/0603161 [quant-ph]].
- [8] S. Chapman, M. P. Heller, H. Marrochio and F. Pastawski, *Phys. Rev. Lett.* **120** (2018) no.12, 121602 doi:10.1103/PhysRevLett.120.121602 [arXiv:1707.08582 [hep-th]].
- [9] V. S. Viswanath, Gerhard Müller, *The recursion method: application to many body dynamics*. Vol. 23. Springer Science and Business Media, 1994.
- [10] D. E. Parker, X. Cao, A. Avdoshkin, T. Scaffidi and E. Altman, *Phys. Rev. X* **9** (2019) no.4, 041017 doi:10.1103/PhysRevX.9.041017 [arXiv:1812.08657 [cond-mat.stat-mech]].
- [11] S. E. Aguilar-Gutierrez and A. Rolph, *Phys. Rev. D* **109** (2024) no.8, L081701 doi:10.1103/PhysRevD.109.L081701 [arXiv:2311.04093 [hep-th]].
- [12] P. Caputa, J. M. Magan and D. Patramanis, *Phys. Rev. Res.* **4** (2022) no.1, 013041 doi:10.1103/PhysRevResearch.4.013041 [arXiv:2109.03824 [hep-th]].
- [13] W. Mück and Y. Yang, *Nucl. Phys. B* **984** (2022), 115948 doi:10.1016/j.nuclphysb.2022.115948 [arXiv:2205.12815 [hep-th]].
- [14] E. Rabinovici, A. Sánchez-Garrido, R. Shir and J. Sonner, *JHEP* **06** (2021), 062 doi:10.1007/JHEP06(2021)062 [arXiv:2009.01862 [hep-th]].
- [15] S. K. Jian, B. Swingle and Z. Y. Xian, *JHEP* **03** (2021), 014 doi:10.1007/JHEP03(2021)014 [arXiv:2008.12274 [hep-th]].
- [16] S. He, P. H. C. Lau, Z. Y. Xian and L. Zhao, *JHEP* **12** (2022), 070 doi:10.1007/JHEP12(2022)070 [arXiv:2209.14936 [hep-th]].
- [17] D. Patramanis, *PTEP* **2022** (2022) no.6, 063A01 doi:10.1093/ptep/ptac081 [arXiv:2111.03424 [hep-th]].
- [18] X. Cao, *J. Phys. A* **54** (2021) no.14, 144001 doi:10.1088/1751-8121/abe77c [arXiv:2012.06544 [cond-mat.stat-mech]].
- [19] F. B. Trigueros and C. J. Lin, *SciPost Phys.* **13** (2022) no.2, 037 doi:10.21468/SciPostPhys.13.2.037 [arXiv:2112.04722 [cond-mat.dis-nn]].
- [20] R. Heveling, J. Wang and J. Gemmer, *Phys. Rev. E* **106** (2022) no.1, 014152 doi:10.1103/PhysRevE.106.014152 [arXiv:2203.00533 [cond-mat.stat-mech]].
- [21] A. Dymarsky and M. Smolkin, *Phys. Rev. D* **104** (2021) no.8, L081702 doi:10.1103/PhysRevD.104.L081702 [arXiv:2104.09514 [hep-th]].
- [22] P. Caputa and S. Datta, *JHEP* **12** (2021), 188 [erratum: *JHEP* **09** (2022), 113] doi:10.1007/JHEP12(2021)188 [arXiv:2110.10519 [hep-th]].
- [23] P. Caputa and S. Liu, *Phys. Rev. B* **106** (2022) no.19, 195125 doi:10.1103/PhysRevB.106.195125 [arXiv:2205.05688 [hep-th]].
- [24] P. Z. He and H. Q. Zhang, [arXiv:2411.16302 [hep-th]].
- [25] P. Z. He and H. Q. Zhang, *JHEP* **11** (2024), 014 doi:10.1007/JHEP11(2024)014 [arXiv:2407.02756 [hep-th]].

- [26] A. Dymarsky and A. Gorsky, Phys. Rev. B **102** (2020) no.8, 085137
doi:10.1103/PhysRevB.102.085137 [arXiv:1912.12227 [cond-mat.stat-mech]].
- [27] B. Bhattacharjee, X. Cao, P. Nandy and T. Pathak, JHEP **05** (2022), 174
doi:10.1007/JHEP05(2022)174 [arXiv:2203.03534 [quant-ph]].
- [28] K. B. Huh, H. S. Jeong and J. F. Pedraza, [arXiv:2312.12593 [hep-th]].
- [29] J. Erdmenger, S. K. Jian and Z. Y. Xian, JHEP **08** (2023), 176
doi:10.1007/JHEP08(2023)176 [arXiv:2303.12151 [hep-th]].
- [30] K. Hashimoto, K. Murata, N. Tanahashi and R. Watanabe, JHEP **11** (2023), 040
doi:10.1007/JHEP11(2023)040 [arXiv:2305.16669 [hep-th]].
- [31] M. J. Vasli, K. Babaei Velni, M. R. Mohammadi Mozaffar, A. Mollabashi and M. Alishahiha,
Eur. Phys. J. C **84** (2024) no.3, 235 doi:10.1140/epjc/s10052-024-12609-9 [arXiv:2307.08307
[hep-th]].
- [32] A. Gill, K. Pal, K. Pal and T. Sarkar, Phys. Rev. B **109** (2024) no.10, 104303
doi:10.1103/PhysRevB.109.104303 [arXiv:2311.07892 [quant-ph]].
- [33] B. Bhattacharjee, P. Nandy and T. Pathak, JHEP **01** (2024), 094
doi:10.1007/JHEP01(2024)094 [arXiv:2311.00753 [quant-ph]].
- [34] K. Adhikari, S. Choudhury and A. Roy, Nucl. Phys. B **993** (2023), 116263
doi:10.1016/j.nuclphysb.2023.116263 [arXiv:2204.02250 [hep-th]].
- [35] T. Q. Loc, [arXiv:2402.07980 [hep-th]].
- [36] P. Caputa, H. S. Jeong, S. Liu, J. F. Pedraza and L. C. Qu, [arXiv:2402.09522 [hep-th]].
- [37] R. Basu, A. Ganguly, S. Nath and O. Parrikar, [arXiv:2402.13694 [hep-th]].
- [38] R. Sasaki, [arXiv:2403.06391 [quant-ph]].
- [39] P. Caputa and K. Kutak, [arXiv:2404.07657 [hep-ph]].
- [40] A. Sahu, [arXiv:2404.09464 [quant-ph]].
- [41] B. Bhattacharjee, S. Sur and P. Nandy, Phys. Rev. B **106** (2022) no.20, 205150
doi:10.1103/PhysRevB.106.205150 [arXiv:2208.05503 [quant-ph]].
- [42] J. Kim, J. Murugan, J. Olle and D. Rosa, Phys. Rev. A **105** (2022) no.1, L010201
doi:10.1103/PhysRevA.105.L010201 [arXiv:2109.05301 [quant-ph]].
- [43] L. Chen, B. Mu, H. Wang and P. Zhang, [arXiv:2404.08207 [quant-ph]].
- [44] B. Bhattacharjee and P. Nandy, [arXiv:2407.07399 [quant-ph]].
- [45] A. Sánchez-Garrido, [arXiv:2407.03866 [hep-th]].
- [46] A. Chattopadhyay, V. Malvimat and A. Mitra, [arXiv:2405.03630 [hep-th]].
- [47] P. Nandy, A. S. Matsoukas-Roubeas, P. Martínez-Azcona, A. Dymarsky and A. del Campo,
[arXiv:2405.09628 [quant-ph]].
- [48] S. Choudhury, S. Chowdhury, N. Gupta, A. Mishara, S. P. Selvam, S. Panda,
G. D. Pasquino, C. Singha and A. Swain, Symmetry **13** (2021) no.7, 1301
doi:10.3390/sym13071301 [arXiv:2012.10234 [hep-th]].
- [49] P. Bhargava, S. Choudhury, S. Chowdhury, A. Mishara, S. P. Selvam, S. Panda and
G. D. Pasquino, SciPost Phys. Core **4** (2021), 026 doi:10.21468/SciPostPhysCore.4.4.026
[arXiv:2009.03893 [hep-th]].

- [50] J. L. Lehnert and J. Quintin, *Phys. Rev. D* **103** (2021) no.6, 063527 doi:10.1103/PhysRevD.103.063527 [arXiv:2012.04911 [hep-th]].
- [51] A. Bhattacharyya, S. Das, S. Shajidul Haque and B. Underwood, *Phys. Rev. D* **101** (2020) no.10, 106020 doi:10.1103/PhysRevD.101.106020 [arXiv:2001.08664 [hep-th]].
- [52] K. Adhikari, S. Choudhury, H. N. Pandya and R. Srivastava, *Symmetry* **15** (2023) no.3, 664 doi:10.3390/sym15030664 [arXiv:2108.10334 [gr-qc]].
- [53] L. H. Liu and A. C. Li, *Phys. Dark Univ.* **37** (2022), 101123 doi:10.1016/j.dark.2022.101123 [arXiv:2102.12014 [gr-qc]].
- [54] A. c. Li, X. F. Li, D. f. Zeng and L. H. Liu, *Phys. Dark Univ.* **43** (2024), 101422 doi:10.1016/j.dark.2024.101422 [arXiv:2102.12939 [gr-qc]].
- [55] T. Li and L. H. Liu, [arXiv:2309.01595 [gr-qc]].
- [56] K. Adhikari and S. Choudhury, *Fortsch. Phys.* **70** (2022) no.12, 2200126 doi:10.1002/prop.202200126 [arXiv:2203.14330 [hep-th]].
- [57] T. Li and L. H. Liu, *JHEP* **04** (2024), 123 doi:10.1007/JHEP04(2024)123 [arXiv:2401.09307 [hep-th]].
- [58] A. Bhattacharya, P. Nandy, P. P. Nath and H. Sahu, *JHEP* **12** (2022), 081 doi:10.1007/JHEP12(2022)081 [arXiv:2207.05347 [quant-ph]].
- [59] T. Li and L. H. Liu, [arXiv:2408.03293 [hep-th]].
- [60] T. Li and L. H. Liu, [arXiv:2405.01433 [hep-th]].
- [61] P. W. Higgs, *Phys. Rev. Lett.* **13** (1964), 508-509 doi:10.1103/PhysRevLett.13.508
- [62] A. A. Starobinsky, *Phys. Lett. B* **91** (1980), 99-102 doi:10.1016/0370-2693(80)90670-X
- [63] A. D. Linde, *Phys. Lett. B* **129** (1983), 177-181 doi:10.1016/0370-2693(83)90837-7
- [64] M. Galante, R. Kallosh, A. Linde and D. Roest, *Phys. Rev. Lett.* **114** (2015) no.14, 141302 doi:10.1103/PhysRevLett.114.141302 [arXiv:1412.3797 [hep-th]].
- [65] A. Albrecht, P. Ferreira, M. Joyce and T. Prokopec, *Phys. Rev. D* **50** (1994), 4807-4820 doi:10.1103/PhysRevD.50.4807 [arXiv:astro-ph/9303001 [astro-ph]].
- [66] D. Baumann, doi:10.1142/9789814327183_0010 [arXiv:0907.5424 [hep-th]].
- [67] L. Kofman, A. D. Linde and A. A. Starobinsky, *Phys. Rev. D* **56** (1997), 3258-3295 doi:10.1103/PhysRevD.56.3258 [arXiv:hep-ph/9704452 [hep-ph]].
- [68] Y. Shtanov, J. H. Traschen and R. H. Brandenberger, *Phys. Rev. D* **51** (1995), 5438-5455 doi:10.1103/PhysRevD.51.5438 [arXiv:hep-ph/9407247 [hep-ph]].
- [69] L. H. Liu and W. L. Xu, *Chin. Phys. C* **44** (2020) no.8, 085103 doi:10.1088/1674-1137/44/8/085103 [arXiv:1911.10542 [astro-ph.CO]].
- [70] L. H. Liu, *Chin. Phys. C* **47** (2023) no.1, 015105 doi:10.1088/1674-1137/ac9d28 [arXiv:2107.07310 [astro-ph.CO]].
- [71] Y. Akrami *et al.* [Planck], *Astron. Astrophys.* **641** (2020), A10 doi:10.1051/0004-6361/201833887 [arXiv:1807.06211 [astro-ph.CO]].
- [72] P. A. R. Ade *et al.* [Planck], *Astron. Astrophys.* **594** (2016), A20 doi:10.1051/0004-6361/201525898 [arXiv:1502.02114 [astro-ph.CO]].

- [73] J. L. F. Barbón, E. Rabinovici, R. Shir and R. Sinha, *JHEP* **10** (2019), 264
doi:10.1007/JHEP10(2019)264 [arXiv:1907.05393 [hep-th]].
- [74] C. Cheung, P. Creminelli, A. L. Fitzpatrick, J. Kaplan and L. Senatore, *JHEP* **03** (2008), 014 doi:10.1088/1126-6708/2008/03/014 [arXiv:0709.0293 [hep-th]].
- [75] B. Bhattacharjee, X. Cao, P. Nandy and T. Pathak, *JHEP* **03** (2023), 054
doi:10.1007/JHEP03(2023)054 [arXiv:2212.06180 [quant-ph]].
- [76] L. H. Liu and T. Prokopec, *JCAP* **06** (2021), 033 doi:10.1088/1475-7516/2021/06/033
[arXiv:2005.11069 [astro-ph.CO]].
- [77] L. H. Liu and W. L. Xu, *Chin. Phys. C* **44** (2020) no.8, 085103
doi:10.1088/1674-1137/44/8/085103 [arXiv:1911.10542 [astro-ph.CO]].
- [78] L. H. Liu, *Chin. Phys. C* **47** (2023) no.1, 015105 doi:10.1088/1674-1137/ac9d28
[arXiv:2107.07310 [astro-ph.CO]].
- [79] X. z. Zhang, L. h. Liu and T. Qiu, *Phys. Rev. D* **107** (2023) no.4, 043510
doi:10.1103/PhysRevD.107.043510 [arXiv:2207.07873 [hep-th]].
- [80] L. H. Liu, T. Prokopec and A. A. Starobinsky, *Phys. Rev. D* **98** (2018) no.4, 043505
doi:10.1103/PhysRevD.98.043505 [arXiv:1806.05407 [gr-qc]].
- [81] L. H. Liu, B. Liang, Y. C. Zhou, X. D. Liu, W. L. Xu and A. C. Li, *Phys. Rev. D* **103** (2021) no.6, 063515 doi:10.1103/PhysRevD.103.063515 [arXiv:2007.08278 [astro-ph.CO]].
- [82] L. H. Liu, doi:10.1007/s10773-018-3809-0 [arXiv:1807.00666 [gr-qc]].
- [83] G. Lindblad, *Commun. Math. Phys.* **48** (1976), 119 doi:10.1007/BF01608499
- [84] V. Gorini, A. Kossakowski and E. C. G. Sudarshan, *J. Math. Phys.* **17** (1976), 821
doi:10.1063/1.522979
- [85] A. Bhattacharyya, T. Hanif, S. S. Haque and A. Paul, *Phys. Rev. D* **107** (2023) no.10, 106007 doi:10.1103/PhysRevD.107.106007 [arXiv:2210.09268 [hep-th]].